IMA Journal of Applied Mathematics (2023) **88**, 805–836
https://doi.org/10.1093/imamat/hxae002
Advance Access publication on 25 January 2024

A bubble model for the gating of K_V channels

ZILONG SONG
Department of Mathematics and Statistics, Utah State University, 3900 Old Main Hill, Logan, 84322 UT, USA

ROBERT EISENBERG
Department of Applied Mathematics, Illinois Institute of Technology, Chicago, 60616 IL, USA
Department of Physiology and Biophysics, Rush University, Chicago, 60612 IL, USA

SHIXIN XU
Zu Chongzhi Center for Mathematics and Computational Sciences, Duke Kunshan University, 8 Duke Ave, Kunshan, Jiangsu 215316, China

AND

HUAXIONG HUANG*
Research Center for Mathematics, Advanced Institute of Natural Sciences, Beijing Normal University, Zhuhai, Guangdong, 519088, China
Guangdong Provincial Key Laboratory of Interdisciplinary Research and Application for Data Science, BNU-HKBU United International College, Zhuhai, Guangdong 519088, China
Department of Mathematics and Statistics, York University, Toronto, ON M3J 1P3, Canada
Laboratory of Mathematics and Complex Systems, MOE, Beijing Normal University, Beijing, 100875, China
*Corresponding author: hhuang@yorku.ca

[Received on 15 October 2022; revised on 8 November 2023; accepted on 2 January 2024]

Voltage-gated K_V channels play fundamental roles in many biological processes, such as the generation of the action potential. The gating mechanism of K_V channels is characterized experimentally by single-channel recordings and ensemble properties of the channel currents. In this work, we propose a bubble model coupled with a Poisson–Nernst–Planck (PNP) system to capture the key characteristics, particularly the delay in the opening of channels. The coupled PNP system is solved numerically by a finite-difference method and the solution is compared with an analytical approximation. We hypothesize that the stochastic behaviour of the gating phenomenon is due to randomness of the bubble and channel sizes. The predicted ensemble average of the currents under various applied voltage across the channels is consistent with experimental observations, and the Cole–Moore delay is captured by varying the holding potential.

Keywords: voltage-gated channels; Poisson–Nernst–Planck system; bubble model; Cole–Moore delay.

1. Introduction

Voltage-gated ion channels play fundamental roles in many biological activities, such as signal generation and propagation in the nervous system, pacemaker activity in the heart, and coordination of contraction in skeletal muscle (Biel *et al.*, 2009; Jacobson *et al.*, 2010; Jensen *et al.*, 2012). For example, the voltage-gated Na (Na_V) and K (K_V) channels are key players in the generation of action potential (AP) signals in the nervous system (Hille, 2001), cardiac and skeletal muscle. This rapid and transient change of

© The Author(s) 2024. Published by Oxford University Press on behalf of the Institute of Mathematics and its Applications. All rights reserved.

Downloaded from https://academic.oup.com/imamat/article/88/5/805/7589766 by guest on 28 March 2024

membrane potential propagates long distances (metres) in the nervous system and muscle fibres as well. The opening and closing of ion channels as the voltage changes across the membrane determine the depolarization (positive change of membrane potential) and repolarization (negative change of membrane potential) that form the propagating AP (Huxley, 1963; Hodgkin, 1992; Huxley, 1996, 2002).

The opening of ion channels follows the change in voltage with a delay and that delay is an important determinant of the conduction velocity of AP. The conduction velocity helps determine how fast the nervous system can function. Therefore, understanding the mechanism of delay is of great biological importance. One of the objectives of the present work is to model the delay in the opening of single K_v channels as well as their ensemble properties. It is not unreasonable to expect that the delay is set by a process that is optimized as much as possible within the constraints of physics, protein structure and evolutionary history (Gould, 1987).

Hodgkin and Huxley (HH) provided an empirical model of the generation of AP in 1952 (Hodgkin & Huxley, 1952). The conductances they used are ensemble averages of those from many channels. Understanding the molecular mechanisms that produce these conductances and the AP is one of the main goals of biophysics for the past 70 years. Recent advances in structural biology (MacKinnon) and single-channel recording (Neher, 1997) have catalyzed our understanding of the physical mechanisms that produce these conductances. The ionic basis of selective conduction is now understood reasonably well for sodium channels (Boda *et al.*, 2007; Dudev & Lim, 2010, 2014; Lim & Dudev, 2016).

The opening and closing of voltage-dependent channels involves many steps (Bezanilla, 2008a; Bezanilla, 2008b). Some of the steps in the voltage-dependent gating of K_v are now known in molecular and physical detail (Bezanilla, 2002; Kim & Warshel, 2014; Lacroix *et al.*, 2014; Horng *et al.*, 2016; Catacuzzeno *et al.*, 2020b, 2021a). The first step is the response of the voltage sensor to the voltage change, and significant progress has been made in understanding the physics of that response. It is plausible (Hodgkin & Huxley, 1952) that the permeability changes depend on the presence of voltage sensors in the form of charged or dipole particles, as suggested earlier in a different form (Hodgkin *et al.*, 1949; Huxley, 2002). The second step is the communication of the voltage sensor with the conduction pore of the channel. The gating phenomenon was revealed experimentally in the single-channel ON-OFF currents (that occur at random intervals) measured by bilayer or patch-clamp experiments from one channel protein at a time (Sakmann & Neher, 1995; Zheng & Trudeau, 2015). The development of patch-clamp experiments (Hamill *et al.*, 1981) was a breakthrough in the understanding of the gating mechanisms and provided experimental verification at high resolution of many studies and models.

In the patch-clamp experiments, the recordings of single K_v channels showed a delay of currents in response to a step voltage change. The ionic current was generated rapidly after the delay, and vanished when the channel closed suddenly (Llano & Bookman, 1986; Llano *et al.*, 1988; Hille, 2001; Werry *et al.*, 2013). The recordings also showed that the delays varied in each ON-OFF experiment: the gating transitions are stochastic. The ensemble average has a smoother transient time course for the currents (or opening and closing of channels), which resembles the classical macroscopic currents (or voltage-dependent conductances) in the HH model.

The delay in opening was first studied in the inaugural issue of the Biophysical Journal (Cole & Moore, 1960) in the ensemble of channels. Cole and Moore were able to control the resting potential (i.e. their holding potential) present before the AP mechanism was turned on. The earlier work of HH had not addressed this issue in detail because the actual resting potential of their squid nerve was substantially different from that used as a holding potential (Moore & Cole, 1960). Hodgkin and Huxley chose to use nerve fibres with more positive resting potentials so their voltage clamp system could control the voltage throughout the nerve fibre, something not easy to do (Taylor *et al.*, 1960). Cole and Moore found the delay in the response of the nerve fibre to a change in voltage was much larger when the initial potential (also called the holding potential) was more negative.

Downloaded from https://academic.oup.com/imamat/article/88/5/805/7589766 by guest on 28 March 2024

Given the importance of this delay (we call the Cole–Moore delay), it is striking that a molecular scale biophysical explanation has not been developed (Hoshi & Armstrong, 2015), as far as we know, until very recently (Priest *et al.*, 2021). Given the obvious evolutionary disadvantage of additional delay, it seems likely that whatever is responsible for the delay is an essential component of the ionic channels that create the AP. We expect the cause of the Cole–Moore delay to be found in many channel types where it has not been investigated in detail.

The amount of work on channel proteins that produce the AP has increased spectacularly in the last decades. The most important single advance (from a biophysical point of view) is the ON-OFF properties of the single channels, that in ensemble produce the delay. Many researchers have proposed that the ON-OFF property arises from the collapse of a bubble. When the single-channel current is zero, a region of the conduction pore acts as a hydrophobic gate (Aryal *et al.*, 2015) that excludes water and ions from that region of the protein, forming a dewetted region, which is known as a bubble. It is believed that the hydrophobic gating plays a critical role in understanding the ion channel permeation and gating (Beckstein & Sansom, 2003, 2004; Jensen *et al.*, 2010, 2012). Direct evidence for the existence of bubbles is emerging as structural biologists exploit the magnificent capabilities of modern techniques of X-ray crystallography and cryoelectron microscopy (Aryal *et al.*, 2015; Langan *et al.*, 2020).

Various modeling efforts have been devoted to understanding the gating mechanisms of K_V channels (Catacuzzeno *et al.*, 2020a). In the early years, kinetic models (or called Markov models) were used for channel gating, by assuming the voltage sensor has multiple subunits which make transitions between different states (Tytgat & Hess, 1992; Bezanilla *et al.*, 1994; Schoppa & Sigworth, 1998). Formally, such kinetic models have some similarity to HH's, as the four *n*-gates in the HH model can be interpreted as four independent subunits that control the gating (Hille, 2001). Such models have been able to predict some important features of the gating mechanism of K_V channels (e.g. Shaker channel) and to fit experimental data, but could not reveal much about the physics of the gating process. With the availability of more structural information about channels and advances in computing power, quantitative models using molecular dynamics (MD) have been developed in recent decades (Delemotte *et al.*, 2011; Jensen *et al.*, 2012; Delemotte *et al.*, 2017). MD simulations incorporating physical laws and interactions of atoms provide insights into the movement of the voltage sensors, intermediate states, and closure of the pore (forming a dewetted region). However, the MD approach is limited by the timescale of the simulations, resolving events in the timescale of 10^{-15}s, and the total simulation length is orders of magnitude lower than the timespan (e.g. 10^{-3} s) of experimentally or biologically relevant processes. This makes it difficult to directly validate the MD results by using the macroscopic currents in experiments. To overcome these limitations, alternative multiscale or macroscopic models (Dryga *et al.*, 2012; Peyser & Nonner, 2012; Kim & Warshel, 2014; Horng *et al.*, 2019) have been developed with reasonable approximations. Some models are based on the formulation of Brownian dynamics, where the voltage sensor is treated as a Brownian particle (Catacuzzeno & Franciolini, 2019). Brownian models are able to predict macroscopic gating currents, where the free parameters involved have been estimated based on multiscale modeling approaches (Catacuzzeno *et al.*, 2021b).

Here we take a different approach. Following the previous hypothesis of the hydrophobic region, we construct a specific macroscopic model of a bubble within the framework of Poisson–Nernst–Planck (PNP) systems and show how it produces the time course of single K_V channels and the ensemble properties, including the Cole–Moore delay. The PNP system and its variants have been found successful in modeling and simulation of many biological processes (Eisenberg & Liu, 2007; Song *et al.*, 2018; Horng *et al.*, 2019; Song *et al.*, 2019; Cao *et al.*, 2020; Song *et al.*, 2020; Zhang & Liu, 2020), such as current-voltage curves through ion channels, the selectivity of ion channels, and ion transport processes in the cell and tissue scales. In this work, a bubble is assumed to be present in the pore (or filter) region of the K_V channel, due to the structural and physical properties of the channel. In the bubble, ions are

Downloaded from https://academic.oup.com/imamat/article/88/5/805/7589766 by guest on 28 March 2024

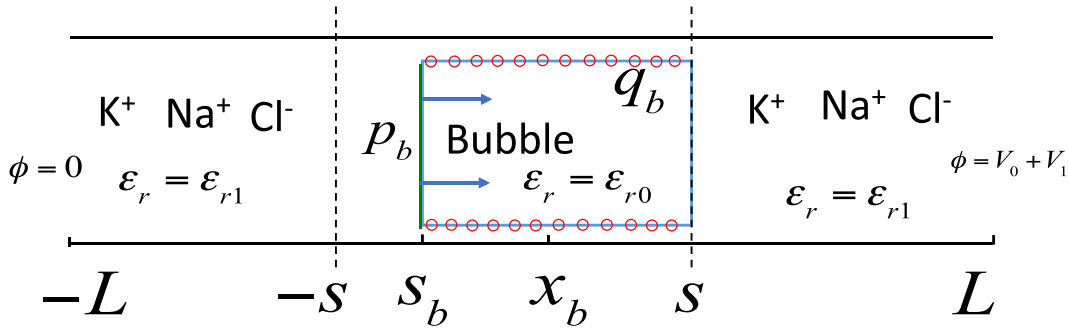

FIG. 1. Sketch of the K_v channel with a bubble in the middle region. The middle bubble centred at x_b blocks the channel before it collapses. The effective charge on the bubble is q_b, indicated by the red circles. There is a dipole moment with strength p_b on the left bubble interface, indicated by the green line The voltages on the two ends are set as $\phi(-L) = 0$ and $\phi(L) = V_0 + V_1$ during the dynamics of bubble, where V_0 is the initial holding potential and V_1 is the voltage jump (elevated).

not present and so cannot carry charge through it, whereas outside the bubble, ion transport is governed by the PNP system. The model is constructed so it can easily accommodate more specific structural information such as the shape, permanent charge (e.g. the spatial distribution of acid and base residue side chains) and dielectric properties of the channel. We calculate the properties of a single channel containing a bubble and an ensemble average based on a simple statistical distribution of such channels to represent the macroscopic currents usually recorded in studies of the opening and closing of channels. This average does not depend on models (Colquhoun & Hawkes, 1981, 1995) of single-channel kinetics. It only assumes that the opening of each channel is independent of the others (because channels are many Debye lengths apart, shielded by the ions, water dipoles, and the ionic atmosphere of proteins and lipid bilayer).

This manuscript is arranged as follows. Section 2 sets up the bubble model within the framework of PNP systems, followed by a non-dimensionalization. In Section 3, the results for a single channel are presented. The bubble model is solved by a finite-difference method and also solved with analytical approximations. The results for the profiles of quantities in the model and the macroscopic currents through the channel are cross-validated by both methods. Section 4 shows the results for ensemble properties of the K_v channels and the Cole–Moore delay, with certain assumptions on the statistical distributions of the bubble locations and cross-sectional area of the channel. Finally, some concluding remarks are provided in Section 5.

2. A bubble model for a voltage-gated Potassium channel

2.1 *The model setup*

We consider a voltage-gated Potassium (K_v) channel in one spatial dimension, as shown in Fig. 1. The total length of channel is set as $2L$, and the length of the middle (filter and pore) region is $2s$. The positions $x = \pm s$ are the locations of the two edges of the middle region. The bubble, together with negative charge $q_b < 0$, can occupy all or part of it, and is centred at $x = x_b$. We assume that the charge is uniformly distributed inside the bubble. The left chamber is connected to a bath environment similar to the exterior of a cell, while the right chamber is connected to one similar to interior of a cell. We anticipate that when the voltage at the right end of the channel is elevated, the bubble shrinks and moves to the right. We assume that the right interface of the bubble is fixed at $x = s$ and the left interface $x = s_b = -s + 2x_b$ is mobile. When the left and right interfaces coincide, the bubble vanishes.

Downloaded from https://academic.oup.com/imamat/article/88/5/805/7589766 by guest on 28 March 2024

REMARK 1. We represent the complex charges in the pore and bubble as an effective charge q_b on the bubble in this one-dimensional low-resolution model. The effective negative charge here is a lumped property of the channel from various effects in a high-dimensional setting, such as the charges from the channel protein (e.g. the residue side chains), differences in dielectric properties of channel wall and pore region, and channel's conformational changes during the bubble dynamics. More detailed formulations will be left for future study with a general bubble shape in a high-dimensional setting.

We consider the case with three ions species K^+, Na^+ and Cl^- (called the major bio-ions) outside of the bubble, and the ions can not penetrate into the bubble (due to energy barriers and the nature of hydrophobic gate). Outside of the bubble, the PNP system is used to model ion transport:

$$\begin{aligned} &-\varepsilon_0 \frac{\partial}{\partial x}\left(\varepsilon_{r1}\frac{\partial}{\partial x}\phi(x,t)\right) = e_0(C_1(x,t)+C_2(x,t)-C_3(x,t)), \quad -L<x<s_b,\ s<x<L,\\ &\frac{\partial C_i(x,t)}{\partial t} = -\frac{\partial}{\partial x}J_i(x,t) = D_i\frac{\partial}{\partial x}\left(\frac{\partial}{\partial x}C_i(x,t)+\frac{e_0 z_i}{k_B T}C_i(x,t)\frac{\partial}{\partial x}\phi(x,t)\right), \quad i=1,2,3, \end{aligned} \tag{2.1}$$

where C_1, C_2 and C_3 are the concentrations (with unit mM) of K^+, Na^+ and Cl^- with valences $z_1 = 1$, $z_2 = 1$ and $z_3 = -1$, ϕ is the electric potential (with unit V), D_i $(i = 1, 2, 3)$ are diffusion coefficients (see Appendix A), $\varepsilon_{r1} = 40$ is the dielectric constant outside of the bubble, and the constants $\varepsilon_0, e_0, k_B, T$ are given by

$$\begin{aligned} &k_B = 1.38\times10^{-23}\,\mathrm{J/K}, \quad e_0 = 1.602\times10^{-19}\,\mathrm{C}, \quad \varepsilon_0 = 8.854\times10^{-12}\,\mathrm{C/(V\cdot m)},\\ &T = 292.15\,\mathrm{K}, \quad k_BT/e_0 \approx 25.17\,\mathrm{mV}, \end{aligned} \tag{2.2}$$

Inside the bubble, we have

$$-\varepsilon_0\frac{\partial}{\partial x}\left(\varepsilon_{r0}\frac{\partial}{\partial x}\phi(x,t)\right) = \frac{q_b}{V_b}, \quad s_b(t)<x<s, \tag{2.3}$$

where $V_b = (s - s_b)A$ is the volume of the bubble, A is the cross-sectional area for the bubble region and is assumed to be a constant $A = (0.7\,\mathrm{nm})^2$, and $\varepsilon_{r0} = 2$ is the dielectric constant inside the bubble.

In addition, we assume that there exists a dipole on the left interface of the bubble $x = s_b$, responsible for maintaining a voltage difference on the two sides of the bubble. Since the membrane potential is not 0 at equilibrium, the presence of the dipole with a suitable dipole strength p_b guarantees that the bubble is in equilibrium initially. The dipole strength p_b is introduced to reflect some effects of curved bubble interfaces in high-dimensional formulation, such as approximation of the Maxwell stress. We can rewrite the equation of ϕ in a compact form in the entire domain $-L < x < L$:

$$-\varepsilon_0\frac{\partial}{\partial x}\left(\varepsilon_r(x,t)\frac{\partial}{\partial x}\phi(x,t)\right) = e_0(c_1(x,t)+c_2(x,t)-c_3(x,t)) + \frac{q_B(x,t)}{V_b} + p_b\frac{\partial}{\partial x}(\delta(x-s_b)), \tag{2.4}$$

Downloaded from https://academic.oup.com/imamat/article/88/5/805/7589766 by guest on 28 March 2024

with the following functions in a piecewise form

$$\varepsilon_r(x,t) = \begin{cases} \varepsilon_{r0}, & [s_b, s], \\ \varepsilon_{r1}, & \text{others}, \end{cases} \quad c_i(x,t) = \begin{cases} 0, & [s_b, s], \\ C_i(x,t), & \text{others}, \end{cases} \quad q_B(x,t) = \begin{cases} q_b, & [s_b, s], \\ 0, & \text{others}, \end{cases} \tag{2.5}$$

where the dependence of ε_r and q_B on t is through the quantity $s_b(t)$.

The total electric force on the bubble is

$$\int_A \int_{s_b}^{s} \frac{q_b}{V_b} \left(-\frac{\partial}{\partial x} \phi(x,t) \right) dx dA = -q_b \frac{\phi(s,t) - \phi(s_b,t)}{s - s_b}, \tag{2.6}$$

then the motion of the bubble is modelled by

$$\frac{dx_b}{dt} = -\frac{q_b D_b}{k_B T} \frac{\phi(s,t) - \phi(s_b,t)}{s - s_b}, \tag{2.7}$$

where D_b ($\ll D_i$) is the diffusion coefficient of the bubble. Here combined coefficient $\frac{q_b D_b}{k_B T}$ is considered as the reciprocal of frictional coefficient for the bubble motion, and the total electric force is the driving force balancing the friction between the bubble and channel wall. Using the relationship $s_b = -s + 2x_b$, we can rewrite equation (2.7) as

$$\frac{ds_b}{dt} = -\frac{2q_b D_b}{k_B T} \frac{\phi(s,t) - \phi(s_b,t)}{s - s_b}. \tag{2.8}$$

The boundary conditions at the two ends are given by

$$\begin{aligned} &\phi(-L,t) = 0, \quad \phi(L,t) = V_0 + V_1 H(t - t_1), \\ &c_i(-L,t) = c_i^L, \quad c_i(L,t) = c_i^R, \end{aligned} \tag{2.9}$$

where V_0 is the initial (holding) membrane potential when the bubble is in equilibrium (or resting state), V_1 is the voltage jump at $t = t_1$, $H(t)$ is a Heaviside function, and c_i^L and c_i^R ($i = 1, 2, 3$) are given bath concentrations at the left and right ends (Llano *et al.*, 1988), which are electro-neutral. In the experiment, the holding potential V_0 is not the same as the Nernst potential of K^+. The leak current is allowed to flow through a different pathway while maintaining V_0.

At the two interfaces $x = s_b$ and s, the electric potential and electric displacement are continuous, and there is no ionic flux across the bubble interfaces (boundary surface for ions). Mathematically, the interface conditions for ϕ and boundary conditions for c_i are given by

$$[\phi] = 0, \quad \left[\varepsilon_r(x,t) \frac{\partial}{\partial x} \phi(x,t) \right] = 0, \quad J_i = 0, \ (i = 1, 2, 3), \quad \text{at} \quad x = s_b, s \tag{2.10}$$

where square brackets mean the jump across the interface, e.g. $[\phi(s,t)] = \phi(s+,t) - \phi(s-,t)$. Alternatively if we include the effect of dipole (p_b in equation 2.4) on the interface rather than in the equation, we obtain a non-zero jump $[\phi]$ at $x = s_b$. When the two interfaces coincide (i.e. $s_b = s$), the

Downloaded from https://academic.oup.com/imamat/article/88/5/805/7589766 by guest on 28 March 2024

bubble collapses. We assume that the dipole disappears (i.e. it is treated as an intrinsic property of the bubble) and the interface conditions are replaced by continuity conditions

$$[\phi] = 0, \quad \left[\varepsilon_r(x,t)\frac{\partial}{\partial x}\phi(x,t)\right] = 0, \quad [c_i] = 0, \quad [J_i] = 0, \ (i = 1,2,3), \quad \text{at} \quad x = s. \tag{2.11}$$

The initial condition for ϕ and c_i at $t = 0$ is set as

$$\begin{aligned} &\phi(x,0) = 0, \quad -L < x < L, \\ &c_i(x,0) = \begin{cases} c_i^L & -L < x < s_b = -s, \\ 0, & s_b < x < s, \\ c_i^R, & s < x < L, \end{cases} \end{aligned} \tag{2.12}$$

where $i = 1,2,3$. This initial condition will be used to compute the initial equilibrium profiles of $\phi(x,t)$ and $c_i(x,t)$ with fixed initial interface position $s_b = s_{b0}$. Then, at $t = t_1$, the voltage jump V_1 is turned on, and the above initial equilibrium profiles are used as initial conditions at $t = t_1$ for the whole system including the dynamics of the bubble with initial condition

$$s_b(t_1) = s_{b0}. \tag{2.13}$$

In summary, we have a system of equations for ion transport coupled with the motion of the bubble, given by (2.4), $(2.2)_2$ and (2.8), together with boundary and interface conditions (2.9, 2.10, 2.11). The total current is conserved in this model, by including three different forms of current, given in Appendix B. This is a special case of the continuity of total current for Maxwell equations (Eisenberg *et al.*, 2017, 2018), and is also similar to the case of a PNP system for electric eels (Song *et al.*, 2020).

REMARK 2. If the dipole does not vanish (i.e. it is treated as property of the channel or channel wall) after the bubble collapses, we will have non-zero jump $[\phi]$ related to the dipole, and $[c_i] = 0$ is replaced by continuity of electro-chemical potential.

2.2 *Non-dimensionalization*

In this subsection, we non-dimensionalize our model, which will be used in the calculations in the subsequent sections. We adopt the following scales:

$$\begin{aligned} &\tilde{x} = \frac{x}{L}, \quad \tilde{s} = \frac{s}{L}, \quad \tilde{x}_b = \frac{x_b}{L}, \quad \tilde{V}_b = \frac{V_b}{LA}, \quad \tilde{\phi} = \frac{\phi}{k_BT/e_0}, \quad \tilde{V}_0 = \frac{V_0}{k_BT/e_0}, \quad \tilde{V}_1 = \frac{V_1}{k_BT/e_0}, \\ &\tilde{c}_i = \frac{c_i}{c_0}, \quad \tilde{c}_i^L = \frac{c_i^L}{c_0}, \quad \tilde{c}_i^R = \frac{c_i^R}{c_0}, \quad \tilde{D}_i = \frac{D_i}{D_0}, (i = 1,2,3), \quad \tilde{D}_b = \frac{D_b}{D_0}, \\ &\tilde{p}_b = \frac{p_b}{e_0c_0L^2}, \quad \tilde{q}_b = \frac{q_b}{e_0}, \quad \tilde{t} = \frac{t}{t_0}, \quad t_0 = \frac{L^2}{D_0}, \quad \tilde{J} = \frac{J}{J_0}, \quad J_0 = \frac{D_0c_0}{L}. \end{aligned} \tag{2.14}$$

The typical values in the above scales and the values in boundary conditions of (2.9) are based on Llano *et al.* (1988) and given in Appendix A.

Downloaded from https://academic.oup.com/imamat/article/88/5/805/7589766 by guest on 28 March 2024

Substituting (2.14) into the system in the previous subsection, we obtain a dimensionless system for variables with tilde (like $\tilde{\phi}$). In order to simply the notations, we drop the tilde and use the same quantities (like ϕ) in the dimensionless system. We have the following set of equations in non-dimensional form:

$$\begin{aligned} -\varepsilon\frac{\partial}{\partial x}\left(\varepsilon_r(x,t)\frac{\partial}{\partial x}\phi(x,t)\right) &= c_1(x,t)+c_2(x,t)-c_3(x,t)+\frac{1}{\beta}\frac{q_B(x,t)}{(s-s_b)} \\ &\quad + p_b\partial_x(\delta(x-s_b)), \quad -1<x<1, \\ \frac{\partial c_i(x,t)}{\partial t} = -\frac{\partial}{\partial x}J_i(x,t) &= D_i\frac{\partial}{\partial x}\left(\frac{\partial}{\partial x}c_i(x,t)+z_ic_i(x,t)\frac{\partial}{\partial x}\phi(x,t)\right), \\ &\quad i=1,2,3, \quad -1<x<s_b \text{ and } s<x<1, \end{aligned} \tag{2.15}$$

with ε_r, q_B and c_i $(i=1,2,3)$ defined in the same way as in (2.5). Here the two dimensionless parameters are defined by

$$\varepsilon = \frac{\varepsilon_0 k_B T}{e_0^2 c_0 L^2}, \quad \beta = LAc_0. \tag{2.16}$$

The motion of the bubble is given by

$$\frac{ds_b}{dt} = -2D_b q_b \frac{\phi(s,t)-\phi(s_b,t)}{s-s_b}. \tag{2.17}$$

Boundary conditions are given by

$$\begin{aligned} &\phi(-1,t)=0, \quad \phi(1,t)=V_0+V_1*H(t-t_1), \\ &c_i(-1,t)=c_i^L, \quad c_i(1,t)=c_i^R, \ (i=1,2,3). \end{aligned} \tag{2.18}$$

Interface conditions for ϕ and boundary conditions for c_i at bubble interfaces are

$$[\phi]=0, \quad \left[\varepsilon_r\frac{\partial}{\partial x}\phi\right]=0, \quad J_i=0, (i=1,2,3), \quad \text{at } x=s_b,s. \tag{2.19}$$

After the bubble collapses (for the case that the dipole disappears), we have

$$[\phi]=0, \quad \left[\varepsilon_r\frac{\partial}{\partial x}\phi\right]=0, \quad [c_i]=0, \quad [J_i]=0, (i=1,2,3), \quad \text{at } x=s_b=s. \tag{2.20}$$

The dimensionless initial conditions has the same form as (2.12, 2.13) except that L is replaced by 1.

3. Results for a single channel

We first compute the initial state when the bubble is in equilibrium by solving the system of equations with a numerical method, followed by the results of the non-equilibrium state including the motion of the bubble and time evolution of the concentrations and electric potential. After the bubble collapses,

Downloaded from https://academic.oup.com/imamat/article/88/5/805/7589766 by guest on 28 March 2024

the ionic fluxes reaches a steady state. In addition, we also present the results obtained with reasonable approximations (verified by numerical evidence) for the intermediate quasi-steady states and the final steady state.

3.1 *Initial state and strength of dipole*

We examine the case that the bubble initially occupies the entire filter region and stays at equilibrium, i.e. $s_b = -s$. We write $\phi(x,t)$ in equilibrium state as $\phi(x)$ here. When $V_0 = 0$, the bubble is in equilibrium due to symmetry. If $V_0 \neq 0$, one the other hand, equilibrium is achieved for an appropriate dipole strength p_b.

Near the interface $x = s_b$, the effect of the other terms is small compared the dipole, and equation (2.15) becomes

$$-\varepsilon \left(\varepsilon_r(x)\phi'(x)\right)' = p_b(\delta(x-s_b))', \tag{3.1}$$

and integrating once gives

$$-\varepsilon\varepsilon_r(x)\phi'(x) = p_b\delta(x-s_b) + C. \tag{3.2}$$

By integrating again and taking the limit of $x \to s_b$, we obtain

$$[\phi(s_b)] = -\frac{p_b}{\varepsilon}\left(\frac{1}{2\varepsilon_{r0}} + \frac{1}{2\varepsilon_{r1}}\right). \tag{3.3}$$

Therefore, for a given V_0, we find the following formula for p_b:

$$-\frac{p_b}{\varepsilon}\left(\frac{1}{2\varepsilon_{r0}} + \frac{1}{2\varepsilon_{r1}}\right) = V_0, \tag{3.4}$$

and then the bubble will be in equilibrium as in the symmetric case with $V_0 = 0$.

For the equilibrium profile, the fluxes are 0 and one can not distinguish the effects of the two cations Na^+ and K^+. We can group the two cation species and treat them as a single species. The boundary values for $c_1 + c_2$ and c_3 will be equal, and hence we will have exact symmetry for this equilibrium case. The equilibrium profiles can be determined analytically, and we take $V_0 = 0$ and $p_b = 0$ in the derivation. Since the bubble is in equilibrium, inside the bubble, we have (note $s_b = -s$)

$$\phi(x) = B_1x^2 + \phi(0), \quad B_1 = -\frac{q_b}{4s\varepsilon\varepsilon_{r0}\beta}. \tag{3.5}$$

Taking the derivative and together with interface conditions at $x = s$, we have

$$\varepsilon_{r1}\phi'(s+) = \varepsilon_{r0}\phi'(s-) = \varepsilon_{r0}2B_1s = \frac{-q_b}{2\varepsilon\beta}. \tag{3.6}$$

Downloaded from https://academic.oup.com/imamat/article/88/5/805/7589766 by guest on 28 March 2024

Due to symmetry, we only consider the right chamber region $s < x < 1$. It is easy to verify that the PNP system (2.15) in equilibrium reduces to

$$\varepsilon\varepsilon_{r1}\phi'' = c_3 - (c_1 + c_2) = e^{\phi} - e^{-\phi}, \tag{3.7}$$

where $c_3^R = 1$ has been used. Integrating once gives

$$\frac{1}{2}\varepsilon\varepsilon_{r1}[(\phi'(x))^2 - (\phi'(s+))^2] = e^{\phi} + e^{-\phi} - (e^{\phi_s} + e^{-\phi_s}), \tag{3.8}$$

where $\phi_s = \phi(s)$. Then, by combining with (3.5), we obatin

$$(\phi'(x))^2 = G(\phi) = \left(\frac{q_b}{2\varepsilon\beta\varepsilon_{r1}}\right)^2 + \frac{2}{\varepsilon\varepsilon_{r1}}\left(e^{\phi} + e^{-\phi} - (e^{\phi_s} + e^{-\phi_s})\right), \tag{3.9}$$

which leads to the solution

$$x = \int_{\phi_s}^{\phi} \frac{1}{\sqrt{G(\phi)}} d\phi + s. \tag{3.10}$$

The unknown constant ϕ_s in the solution can be determined by the condition

$$1 = \int_{\phi_s}^{0} \frac{1}{\sqrt{G(\phi)}} d\phi + s. \tag{3.11}$$

REMARK 3. Because of symmetry, we can obtain a good estimate for ϕ_s from the above derivation

$$\phi_s \approx -\ln\left(\frac{q_b^2}{8\varepsilon\varepsilon_{r1}\beta^2}\right) \tag{3.12}$$

for q_b in a certain range. For example, with parameters in the following example, we have $\phi_s = -4.72$ while the above formula gives $\phi_s \approx -4.71$.

For the numerical results obtained in this paper, we vary the potentials at the two ends of the domain while fixing dipole strength as $q_b = -2$. Most of the other parameter values used for the computation are also fixed and given in Appendix A.

In Fig. 2(a), the electric potential ϕ is plotted for the case of $V_0 = 0$. When $V_0 = -3.18$ (i.e. -80 mV), we determine $p_b \approx 0.044$ using (3.4) and the electric potential is plotted in Fig. 2(b), where the jump at the interface $x = s_b$ is due to the presence of the dipole. The concentrations c_1, c_2 and c_3 (which can be computed from solution of ϕ) are shown in Fig. 2(c–e). It can be seen that $c_1 + c_2$ in Fig. 2(d) is symmetric as expected. The initial membrane potential V_0 is balanced by the jump of ϕ due to the presence of the dipole. In the non-equilibrium case (before the bubble collapses), we will ignore both the initial membrane potential V_0 and the dipole, so that the value of ϕ is continuous at the interfaces. The solutions in Fig. 2 will be verified by numerical simulations in the subsequent subsections.

Downloaded from https://academic.oup.com/imamat/article/88/5/805/7589766 by guest on 28 March 2024

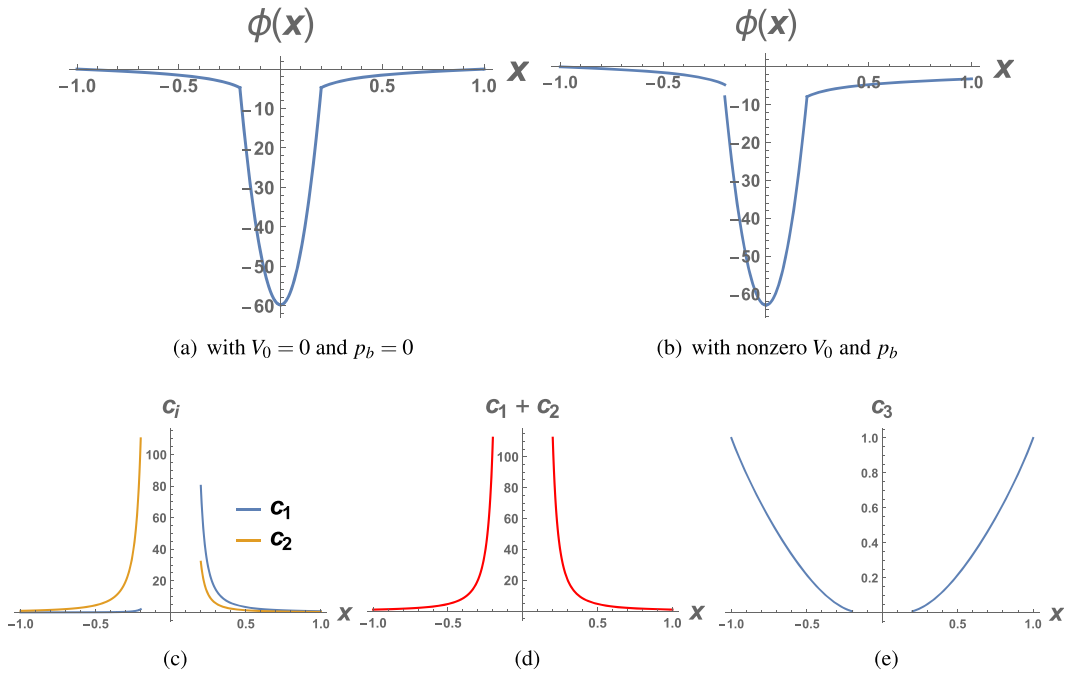

(a) with $V_0 = 0$ and $p_b = 0$ (b) with nonzero V_0 and p_b

(c) (d) (e)

FIG. 2. Equilibrium electric potential ϕ and concentrations c_1, c_2, c_3 when $q_b = -2$.

3.2 *The dynamics of the bubble motion and channel currents*

In this part, we present numerical solutions of the PNP system and bubble motion. Inside the bubble, there exist no ions and their concentrations c_i $(i = 1, 2, 3)$ are zero. For convenience, the PNP system is solved inside the bubble by assigning small diffusion coefficients $(D_1 = D_2 = 10^{-15})$.

The finite difference method is used to solve the system, with a uniform mesh $h = x_k - x_{k-1}$. A temporal semi-implicit discrete scheme is used with $t_n = n\Delta t$ and $x_k = x_0 - kh$, given by

$$
\begin{aligned}
&-\varepsilon\frac{\varepsilon_{r,k-1/2}}{h^2}\phi_{k-1}^{n+1} + \varepsilon\frac{\varepsilon_{r,k-1/2}+\varepsilon_{r,k+1/2}}{h^2}\phi_k^{n+1} - \varepsilon\frac{\varepsilon_{r,k+1/2}}{h^2}\phi_{k+1}^{n+1} - c_{1,k}^{n+1} - c_{2,k}^{n+1} + c_{3,k}^{n+1} = q_k^{n+1},\\
&\frac{c_{i,k}^{n+1} - c_{i,k}^{n}}{\Delta t} = -\frac{J_{i,k+1/2}^{n+1} - J_{i,k-1/2}^{n+1}}{h}, \quad i = 1, 2, 3,\\
&J_{i,k+1/2}^{n+1} = -D_{i,k+1/2}\frac{c_{i,k+1}^{n+1} - c_{i,k}^{n+1}}{h} - D_{i,k+1/2}z_i c_{k+1/2}^{n}\frac{\phi_{k+1}^{n+1} - \phi_k^{n+1}}{h},
\end{aligned}
\tag{3.13}
$$

where harmonic average is used for the diffusion coefficient

$$
D_{i,k+1/2} = \frac{2}{\frac{1}{D_{i,k}} + \frac{1}{D_{i,k+1}}}, \quad i = 1, 2, 3. \tag{3.14}
$$

Downloaded from https://academic.oup.com/imamat/article/88/5/805/7589766 by guest on 28 March 2024

In this way, we ensure that the ionic fluxes are small near the interface as approximations of $J_i = 0$ ($i = 1, 2, 3$). When the bubble collapses, the diffusion coefficient is guaranteed to be the same as that outside of the bubble, and the continuity conditions are recovered. The quantities $\varepsilon_{r,k+1/2}$ and q_k^n in (3.13) are defined in Appendix B. The discrete scheme also preserves the continuity of the total current (given in Appendix B), as in the original continuous model.

For $q_b = -2$, we first compute the initial equilibrium with initial condition in (2.12) when the bubble occupies the entire middle region, i.e. $s_{b0} = -s$. We also set $V_0 = 0$ and $p_b = 0$ in the computation so that ϕ is continuous. The computation is carried out until the system reaches a steady state. For a given mesh size $h = 0.0025$, Fig. 3 shows the numerical solution of electric potential ϕ, concentrations c_i and ionic fluxes J_i ($i = 1, 2, 3$), which are in good agreement with the analytical results in the previous subsection.

Next, we present the results on the bubble motion and dynamic behaviour of the PNP system. We start from the equilibrium state at $t = 0$ and increase the electric potential from 0 to $\phi(1, t) = V_1 = 6.36$ (i.e. 160 mV) for $0 < t < t^*$ (we already set $V_0 = 0$ and $p_b = 0$), where t^* is the unknown time when the bubble collapses. Figure 4 shows ϕ, c_i ($i = 1, 2, 3$) at three different times. The minimum value for ϕ inside the bubble gradually increases in Fig. 4(a), and the interface s_b moves to the right as indicated by Fig. 4. Figure 5 shows the ionic fluxes at three different times, which are small. After the bubble collapses and the dipole disappears, we reset $\phi(1, t) = V_0 + V_1 = 3.18$. Figure 6 shows the three ionic fluxes J_i ($i = 1, 2, 3$) at $x = \pm 1$. It can be seen that they remain small until the bubble collapses (i.e. $s_b = s$) at $t^* = 3.13 \times 10^6$, which is 17.6 ms in dimensional unit. The ionic fluxes and ϕ, c_i ($i = 1, 2, 3$) reach a steady state soon after the bubble collapses, as shown in Fig. 7. At steady state, the dimensionless ionic flux J_1 and the dimensional current I are found to be

$$J_1 \approx -2.834, \quad I = |J_1| e_0 A J_0 \approx 10\,\text{pA}. \tag{3.15}$$

REMARK 4. The value of the steady state current I obtained above is close to that given in Fig. 2(a) of (Llano *et al.*, 1988). When the voltage jump V_1 is reset to 0 after the system reaches a steady state, the ionic fluxes reduce to 0 immediately, indicating the closure of the ion channel. In this sense, our proposed model provides a plausible mechanism for the channel current through the conduction pore once the bubble is generated. However, the mechanism of the bubble generation is not considered here and will be the subject of a future study.

3.3 *Quasi-static equilibrium*

Since the motion of the bubble is extremely slow compared with the diffusive timescale of the ions, ionic fluxes are essentially zero (Fig. 5) before the bubble collapses. Therefore, we can use quasi-static solution with zero ionic fluxes as an approximation of the intermediate states. A hybrid method can be used to determine the solution of intermediate states by first obtaining an analytical solution (in terms of integrals), and then by determining the unknown constants using a numerical method.

Given boundary condition V_1 and interface position s_b, solving the quasi-static equilibrium is similar to that for solving the initial state. Again for a fixed t, we write $\phi(x, t)$ in quasi-static equilibrium as $\phi(x)$ in the following derivation. We set $V_0 = 0$ and $p_b = 0$ so that the continuity condition of ϕ can be used at interface s_b. Inside the bubble, we have

$$\phi(x) = B_1(x - s)^2 + \tilde{\phi}_s(x - s) + \phi_s, \quad B_1 = \frac{-q_b}{2(s - s_b)\varepsilon\varepsilon_{r0}\beta}, \tag{3.16}$$

Downloaded from https://academic.oup.com/imamat/article/88/5/805/7589766 by guest on 28 March 2024

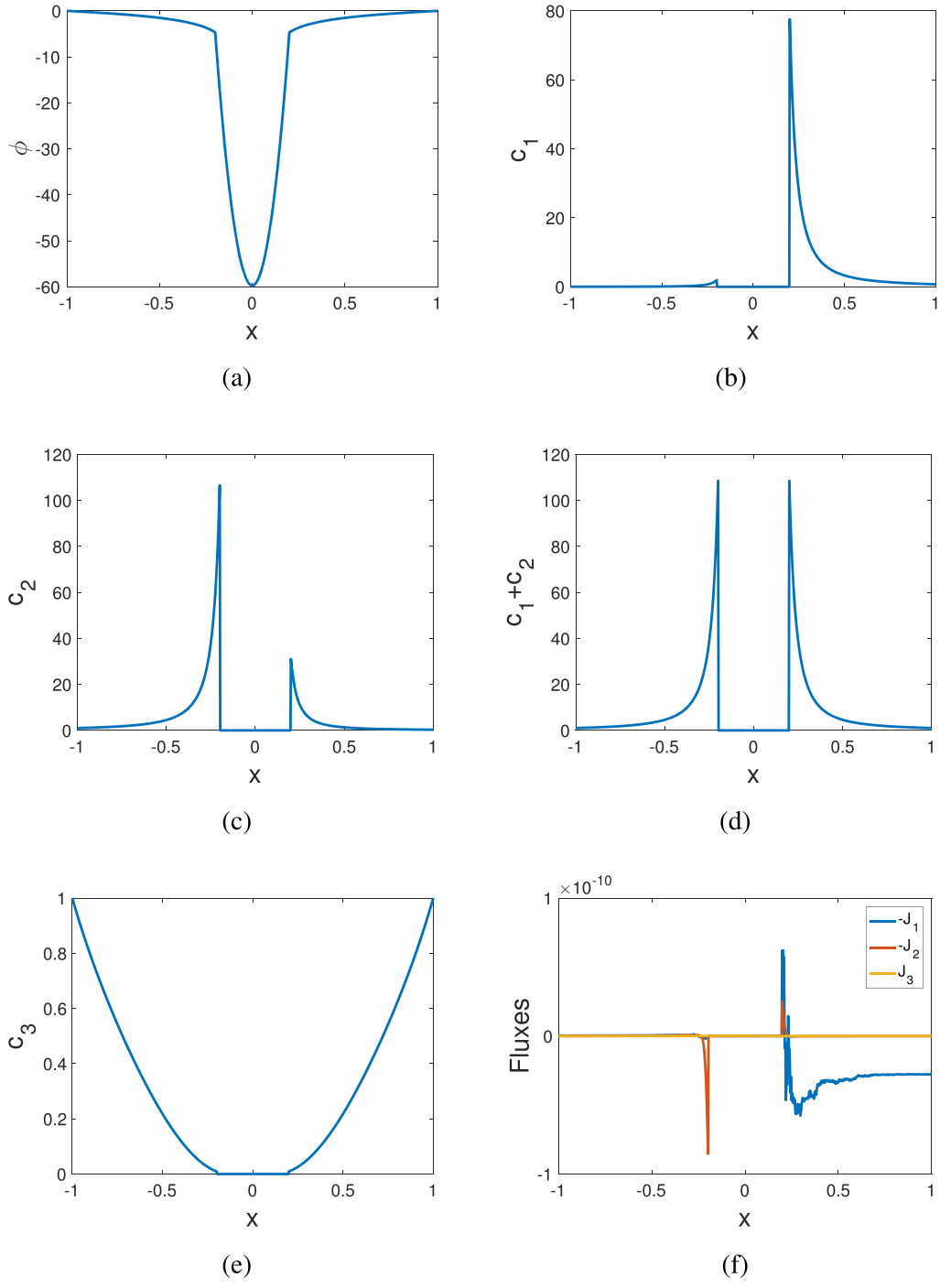

FIG. 3. Equilibrium electric potential ϕ, concentrations c_1, c_2, $c_1 + c_2$, c_3, and ionic fluxes J_i $(i = 1, 2, 3)$ with $h = 0.0025$.

Downloaded from https://academic.oup.com/imamat/article/88/5/805/7589766 by guest on 28 March 2024

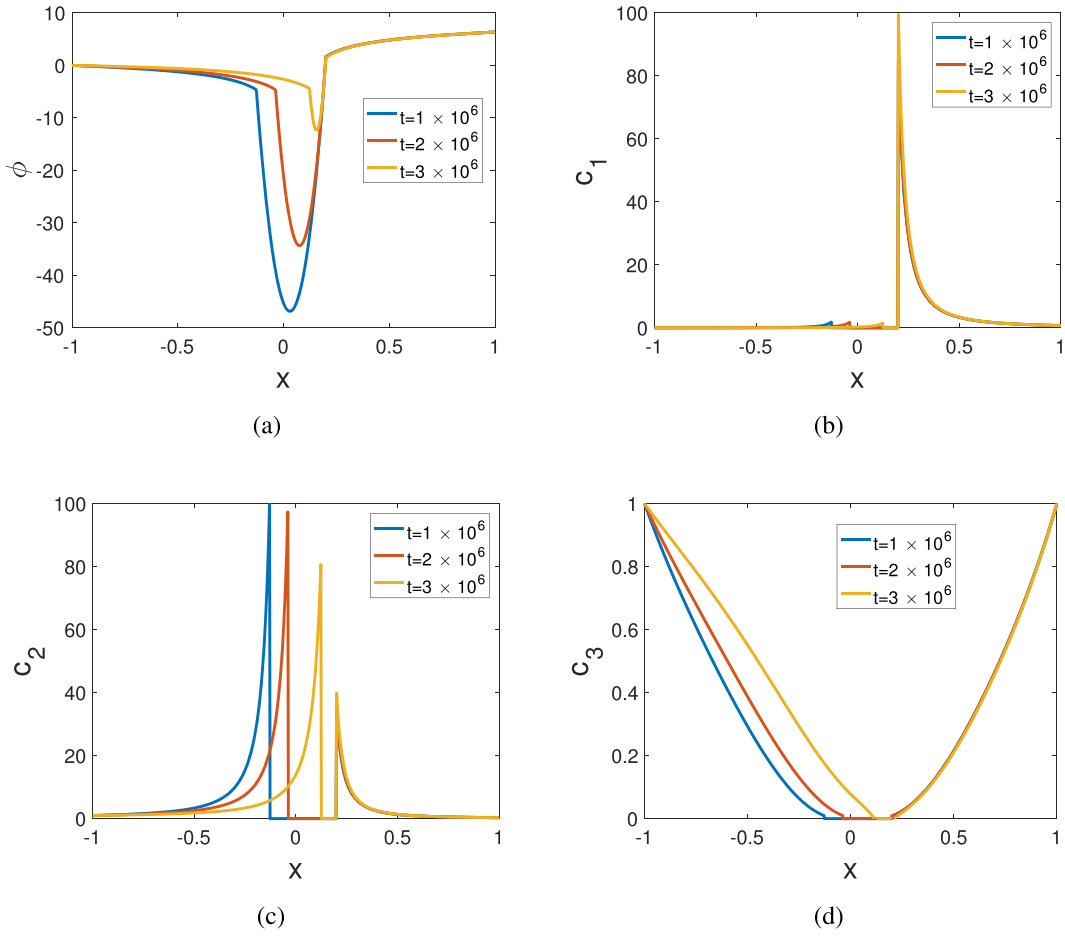

FIG. 4. Electric potential ϕ and ionic concentrations c_1, c_2, c_3 at three different times with $V_1 = 6.36$ during the dynamics of the bubble.

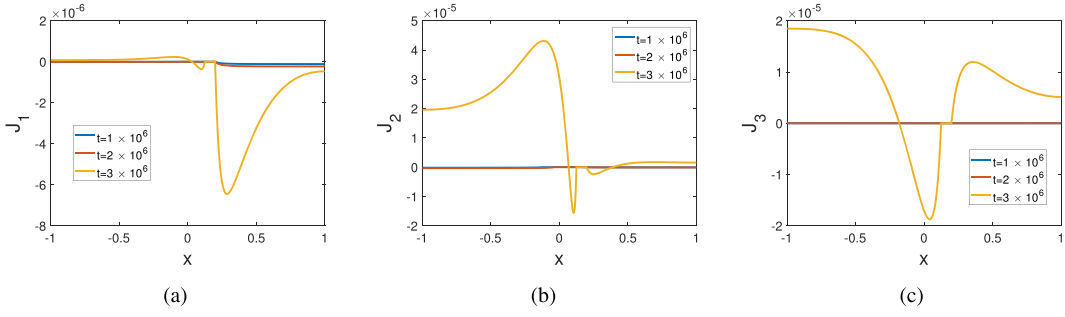

FIG. 5. The fluxes J_i $(i = 1, 2, 3)$ at three different times with $V_1 = 6.36$ during the dynamics of the bubble.

Downloaded from https://academic.oup.com/imamat/article/88/5/805/7589766 by guest on 28 March 2024

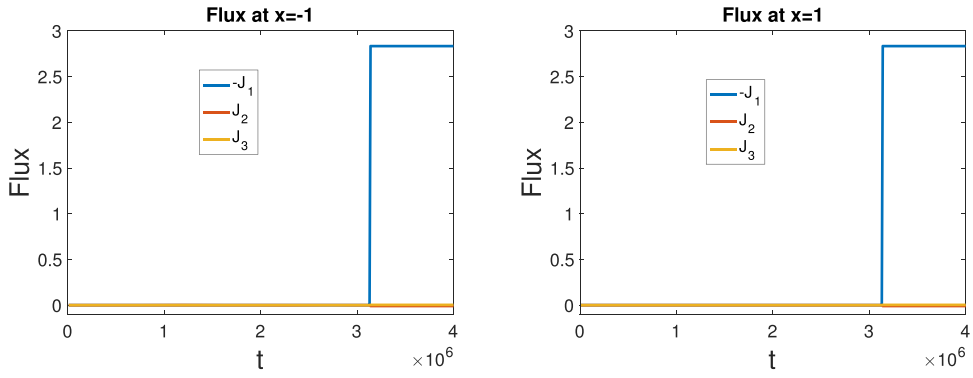

FIG. 6. The dynamics of ionic fluxes J_i ($i = 1, 2, 3$) with $V_1 = 6.36$.

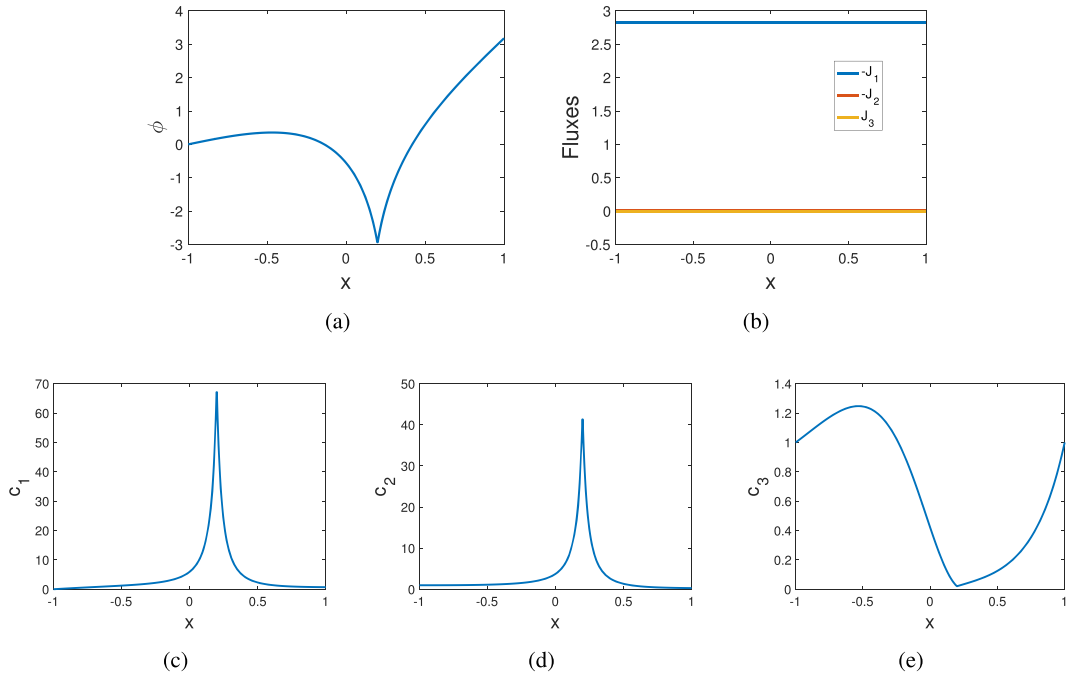

FIG. 7. The electric potential ϕ, the fluxes J_i ($i = 1, 2, 3$), and the concentrations c_1, c_2, c_3 at the steady state with $V_1 = 6.36$ after the bubble collapses.

Downloaded from https://academic.oup.com/imamat/article/88/5/805/7589766 by guest on 28 March 2024

where $\phi_s, \tilde{\phi}_s$ are to be determined. The solutions of ϕ outside of the bubble can be written as

$$\begin{aligned} x &= \int_{\phi_s}^{\phi} \frac{1}{\sqrt{G_1(\phi;\phi_s,\tilde{\phi}_s)}} d\phi + s, \quad s < x < 1, \\ x &= -\int_{\phi_{s_b}}^{\phi} \frac{1}{\sqrt{G_2(\phi;\phi_s,\tilde{\phi}_s)}} d\phi + s_b, \quad -1 < x < s_b, \end{aligned} \tag{3.17}$$

where $\phi_{s_b} = \phi(s_b)$ can be expressed by ϕ_s and $\tilde{\phi}_s$. The derivation for $G_1(\phi), G_2(\phi)$ are given in Appendix C. With given parameter values including V_1 and s_b, the two unknowns ϕ_s and $\tilde{\phi}_s$ can be determined by the two boundary conditions $\phi(1) = V_1$ and $\phi(-1) = 0$, i.e.

$$1 = \int_{\phi_s}^{V_1} \frac{1}{\sqrt{G_1(\phi;\phi_s,\tilde{\phi}_s)}} d\phi + s, \quad -1 = -\int_{\phi_{s_b}}^{0} \frac{1}{\sqrt{G_2(\phi;\phi_s,\tilde{\phi}_s)}} d\phi + s_b, \tag{3.18}$$

and $\phi(x), c_i(x)$ $(i = 1, 2, 3)$ can be obtained afterwards. As an example, for $q_b = -2$, $V_1 = 6.36$ and $s_b = 0$, solution of ϕ and c_i $(i = 1, 2, 3)$ can be computed using the procedure outlined above and plotted in Fig. 8.

For fixed V_1, we can treat $\phi(s), \phi(s_b)$ as functions of parameter s_b, which can be determined by

$$\frac{ds_b}{dt} = -2D_b q_b \frac{\phi(s) - \phi_(s_b)}{s - s_b} = -2D_b q_b f(s_b). \tag{3.19}$$

Note that in the quasi-static case, $\phi(s,t), \phi(s_b,t)$ does not explicitly depend on t, but only depend on s_b (the dependence of $\phi(s,t)$ on t is through $s_b(t)$). Integrating in time, we obtain t^*, the time delay after the voltage jump and before the bubble collapses,

$$t^* = \int_{-s}^{s} \frac{-1}{2D_b q_b f(x)} dx. \tag{3.20}$$

This approximate formula provides a way to fast compute the crucial time delay t^* without solving the dynamics of the whole system.

Figure 9(a) shows the dependence of quantities $\phi(s)$ and $\phi(s_b)$ on s_b, and Fig. 9(b) shows the function $f(s_b)$. From (3.20), we find that $t^* \approx 3.26 \times 10^6$, which is 18.3 ms in dimensional unit, which is slightly longer than that obtained using the finite difference method (17.6 ms) previously.

3.4 *The steady state after the collapse of the bubble*

After the bubble collapses, interface conditions $J_i = 0$ $(i = 1, 2, 3)$ are replaced by continuity conditions $[J_i] = 0$ and q_b becomes a point charge (a delta function). Due to the presence of q_b, the concentration of c_3 is approximately zero near $x = s$, and we assume $J_3/D_3 \approx 0$. We write $\phi(x,t)$ at steady state as

Downloaded from https://academic.oup.com/imamat/article/88/5/805/7589766 by guest on 28 March 2024

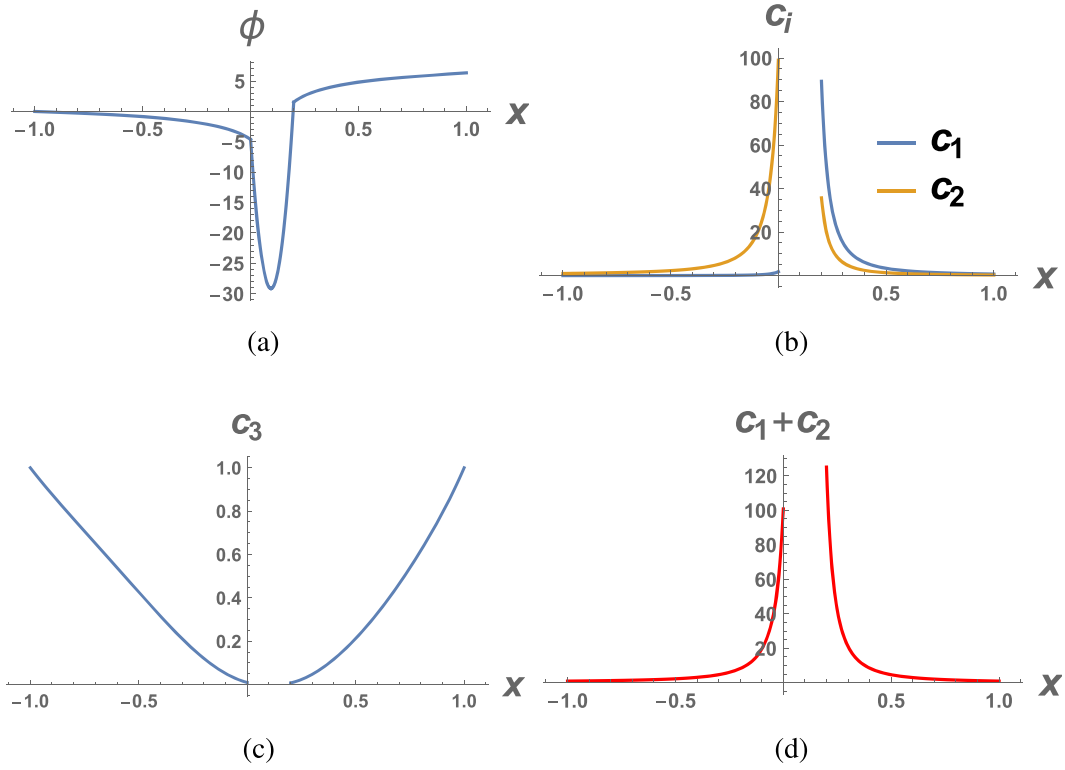

FIG. 8. The quasi-static solution of ϕ, c_1, c_2, c_3 and $c_1 + c_2$ for $s_b = 0$ and $V_1 = 6.36$.

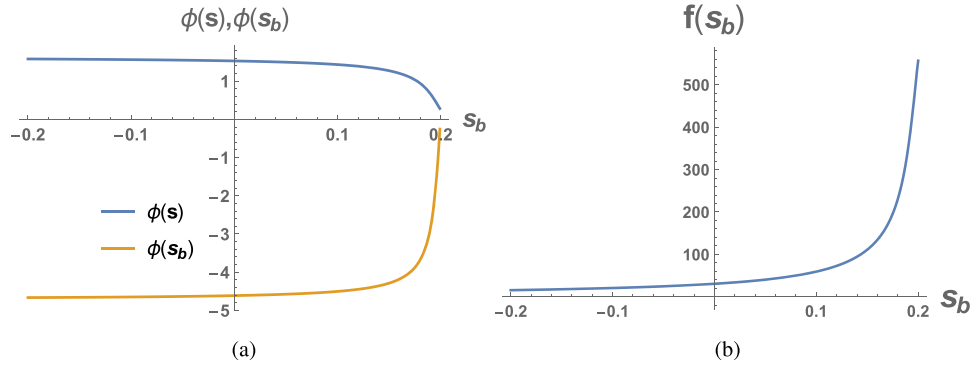

FIG. 9. The dependence of $\phi(s)$ and $\phi(s_b)$ on s_b and function $f(s_b)$ for $V_1 = 6.36$.

Downloaded from https://academic.oup.com/imamat/article/88/5/805/7589766 by guest on 28 March 2024

$\phi(x)$ in the derivation. The system at the steady state can be approximated by

$$\begin{aligned} -\varepsilon\varepsilon_{r1}\phi''(x) &= c_1 + c_2 - c_3 + \frac{q_b}{\beta}\delta(x-s), \\ -J_1 &= c_1' + c_1\phi', \\ -\frac{J_2}{D_2} &= c_2' + c_2\phi', \\ 0 &= c_3' - c_3\phi', \end{aligned} \tag{3.21}$$

where $D_1 = 1$ has been used. If we combine the effect of c_1, c_2 and define $J_p = J_1 + \frac{J_2}{D_2}$, the system can be reduced to a single equation of ϕ (see the derivation in Appendix C)

$$\begin{aligned} -\varepsilon\varepsilon_{r1}\phi''(x) &= \frac{1}{2}\varepsilon\varepsilon_{r1}\left[(\phi'(x))^2 - (\phi'(1))^2\right] - J_p(x-1) - 2(e^{\phi - V} - 1), \quad \text{for} \quad s < x < 1, \\ -\varepsilon\varepsilon_{r1}\phi''(x) &= \frac{1}{2}\varepsilon\varepsilon_{r1}\left[(\phi'(x))^2 - (\phi'(-1))^2\right] - J_p(x+1) - 2(e^{\phi} - 1), \quad \text{for} \quad -1 < x < s, \end{aligned} \tag{3.22}$$

where $V = V_0 + V_1$ and $c_3^L = c_3^R = 1$ have been used. The point charge (delta function) at $x = s$ gives the jump condition

$$[\phi'] = \frac{-q_b}{\beta\varepsilon\varepsilon_{r1}}. \tag{3.23}$$

Given $\phi'(1)$, $\phi'(-1)$, and J_p, the solutions can be easily determined numerically, in the two regions $s < x < 1$ and $-1 < x < s$. The three constants $\phi'(1), \phi'(-1), J_p$ can be determined by condition (3.23), $[\phi] = 0$ and $[c_1 + c_2] = 0$ at $x = s$ (in practice, the numerical procedure is more stable if the ratio $(c_1(s+) + c_2(s+))/(c_1(s-) + c_2(s-)) = 1$ is used instead of $[c_1 + c_2] = 0$). Once $\phi(x)$ is obtained, c_1 and J_1 can be computed by equation $(3.21)_2$ and the continuity condition $[c_1] = 0$ at $x = s$. Similarly, c_2 and J_2 can be computed by equation $(3.21)_3$ and the continuity condition $[c_2] = 0$ at $x = s$.

Figure 10 shows the quasi-static approximations ϕ and c_i $(i = 1, 2, 3)$ at steady state for $V_1 = 6.36$, which agrees with those in Fig. 7 except for c_3. With smaller V_1, the quasi-static approximations are better. For $V_1 = 6.36$, ionic flux J_1 is found to be $J_1 \approx -2.855$ (also ≈ 10 pA in units), which is close to -2.834 in (3.15) obtained by the finite difference method. The advantage of the method in this subsection is that the computation is extremely fast compared with the full finite difference method. It is much more efficient to use the quasi-static approximation to compute the steady states (particularly the currents) with various different voltage jump V_1.

Figure 11 shows the results with $V_1 = 1.59$ (i.e. 40 mV in physical units), and the flux is $J_1 \approx -0.264$ (i.e. 0.933 pA in units). In above computations, J_2 is very small since a small D_2 is used; therefore, the dimensionless total current is almost the same as J_1. Figure 12 shows the dependence of dimensionless flux $-J_1$ and the dimensional current on the voltage $V = V_0 + V_1$ at a steady state (note that the initial holding/equilibrium potential $V_0 = -80$ mV in our calculation).

REMARK 5. In the present simple model, the effective permanent charge is evenly distributed in the bubble only and the size effect of different ions are not considered. We do not expect our model to capture the current-voltage relation for large V_1, including the saturation phenomenon observed experimentally in

Downloaded from https://academic.oup.com/imamat/article/88/5/805/7589766 by guest on 28 March 2024

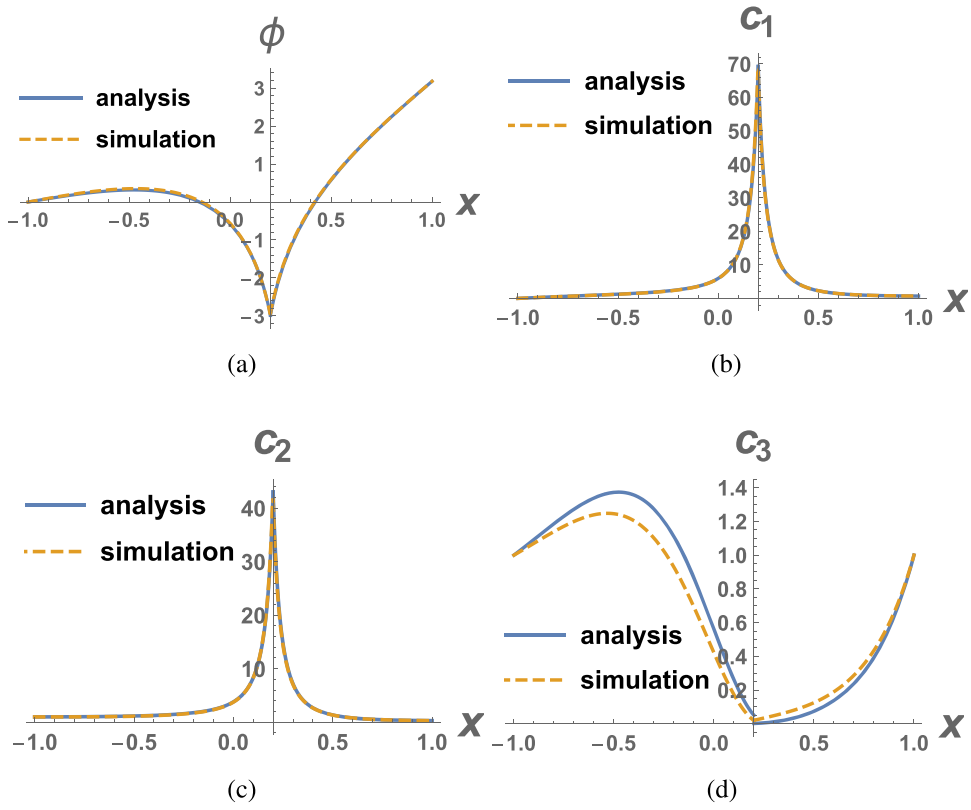

FIG. 10. Comparison of electric potential ϕ and concentrations c_i $(i = 1, 2, 3)$ at steady state with $V_1 = 6.36$ between quasi-static approximation/analysis (solid lines) and the finite difference simulation (dashed lines).

the literature. To make our model more realistic, we need to know the distribution of permanent charge (e.g. acid base side chains) along the system. When that information is available, it can be incorporated into our model by adding permanent charge to the channel wall in the region $-s$ to $+s$ (see Fig. 1) as in a practical implementation (Miedema *et al.*, 2007). The studies (Eisenberg & Liu, 2007; Zhang & Liu, 2020) by Weishi Liu and his group have illustrated the effects of permanent charge on current-voltage relation. With ionic size effect and the permanent charge, saturation phenomenon of current-voltage curves can be modelled as shown in Song *et al.* (2019).

REMARK 6. For the case that the dipole does not disappear after bubble collapses, Fig. 13 shows the results for steady state flux, which are quite similar to those in Fig. 12 for the above case when dipole disappears after bubble collapses.

4. Ensemble properties

In this section, we extend our model by including stochastic effect in two aspects. We assume that the initial position of the bubble and the cross-sectional area of the channel are both random and compute

Downloaded from https://academic.oup.com/imamat/article/88/5/805/7589766 by guest on 28 March 2024

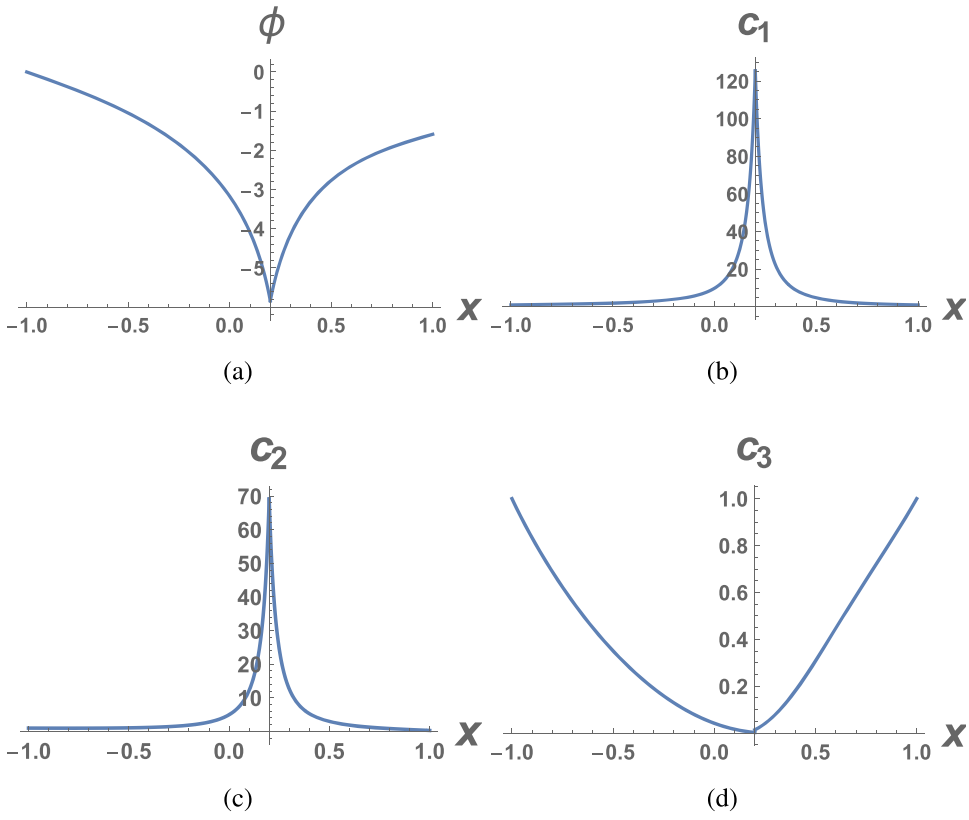

FIG. 11. The electric potential ϕ and the concentrations c_i $(i = 1, 2, 3)$ at the steady state with $V_1 = 1.59$.

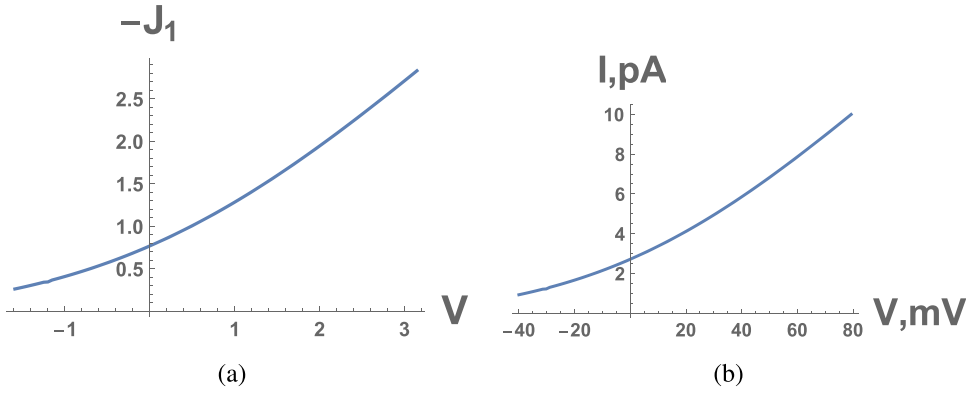

FIG. 12. The dependence of the dimensionless flux J_1 and the dimensional current I on the voltage $V = V_0 + V_1$ at a steady state.

Downloaded from https://academic.oup.com/imamat/article/88/5/805/7589766 by guest on 28 March 2024

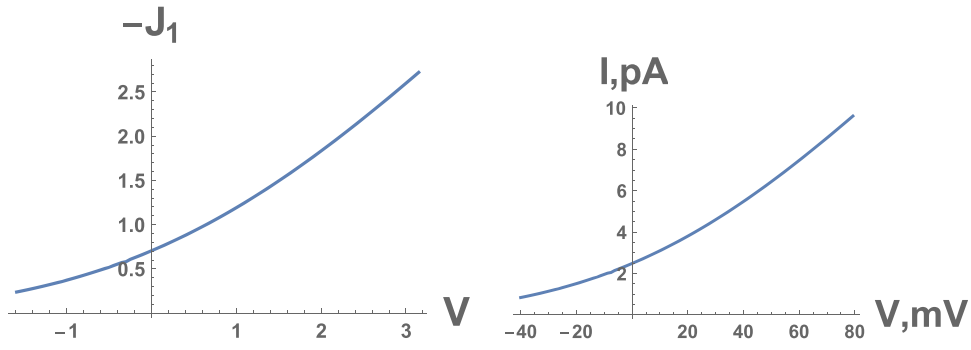

(a) (b)

FIG. 13. The dependence of the dimensional flux J_1 and the dimensional current I on the voltage $V = V_0 + V_1$ at a steady state for the case that the dipole does not disappear after the bubble collapses.

the ensemble averages of the macroscopic currents through the channel and estimate the Cole–Moore delay based on certain statistical distributions.

First, we assume that the initial interface position s_{b0} is random, which could be due to the tiny fluctuations of strength of dipoles in different channels or due to the mechanism of bubble formation (which is not considered in the present work). For illustration, we consider that s_{b0} follows a normal distribution

$$s_{b0} \sim N(\mu, \sigma^2), \quad \mu = 0, \quad \sigma = 0.05, \tag{4.1}$$

where the choice of σ ensures that $s_{b0} \in [-s, s]$ with $s = 0.2$ for almost all the generated data. We can use the previous function $f(s_b)$ to compute the ensemble properties of the channel, since there is negligible effect on the curves of $f(s_b)$ with different starting value of s_{b0}. With each different initial position s_{b0}, the dynamics of the fluxes (particularly the time delay t^* for opening of the channel) will be different. By taking the average of these fluxes, we get the ensemble curve for the dynamics of the current through the channel (i.e. fluxes of K^+). Figure 14(b, c) shows the ensemble curves for the current I and the ratio I/V_1 with 50 channels and with four different voltage jumps that are given in Fig. 14(a). Figure 14(b) shows similar features and scale with experiments in Fig. 2(a, c) in Llano *et al.* (1988).

The case is more complicated when cross-sectional area A is random. We set $A = A_0 A_1$, where $A_1 \sim N(1, \sigma_A^2)$ with $\sigma_A = 0.03$ and $A_0 = (0.7\text{nm})^2$ (the same as the value in Appendix A). The area A will affect the dimensionless parameter β, and hence influences the effective permanent charge q_b/β.

We start by examining the effect of A_1 on t^*. Figure 15 shows $f(s_b)$ with three different values of A_1, indicating that the effect of A_1 on $f(s_b)$ and, hence, on t^* is very small. Therefore, the previous curve $f(s_b)$ can be used to compute t^* as an approximation. Then, we study the effect of A_1 on the flux J_1 or the current I at steady state. Figure 16(a) shows the dependence of J_1 on A_1, indicating that the magnitude of J_1 will slightly decrease with increase of A_1. Since the final dimensional current also depends on the scaling factor which contains A_1, Fig. 16(b) shows the dependence of the current I on the parameter A_1, indicating that the current increases with A_1. Figure 16(b) also shows the approximate current $A_1 I(1)$ where $I(1)$ is taken from previous computation with $A_1 = 1$, which is close to the exact curve. Therefore,

Downloaded from https://academic.oup.com/imamat/article/88/5/805/7589766 by guest on 28 March 2024

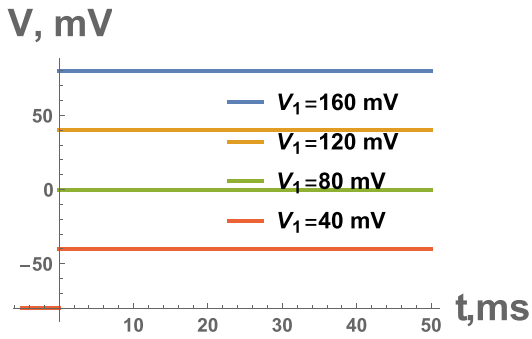

(a) The four voltage jumps V_1 which occurs at $t = 0$

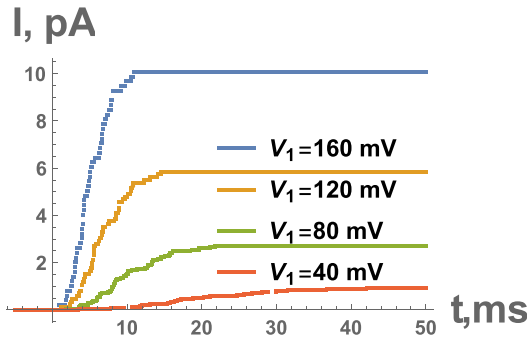

(b) The current I

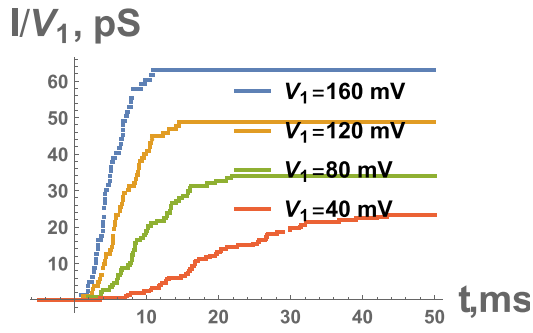

(c) The ratio I/V_1

FIG. 14. The ensemble curves for the current I and the ratio I/V_1 averaged by 50 random s_{b0} and with four different voltage jumps V_1.

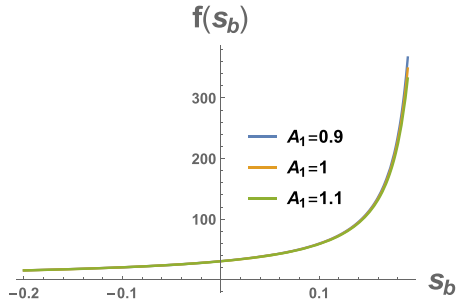

FIG. 15. The function $f(s_b)$ with three values of the parameter A_1.

the main effect of A_1 on the current is due to the scaling factor. We conclude that $A_1 I(1)$ can be used as an approximation for the current in the following figures.

We fix A_1 for each channel during the evolution of the bubble, while allowing it (together with s_{b0}) to vary randomly among 50 channels. The ensemble curves (omitted here) for the current with 50 channels are very similar to those in Fig. 14. We also consider the case that A_1 fluctuates randomly when the

Downloaded from https://academic.oup.com/imamat/article/88/5/805/7589766 by guest on 28 March 2024

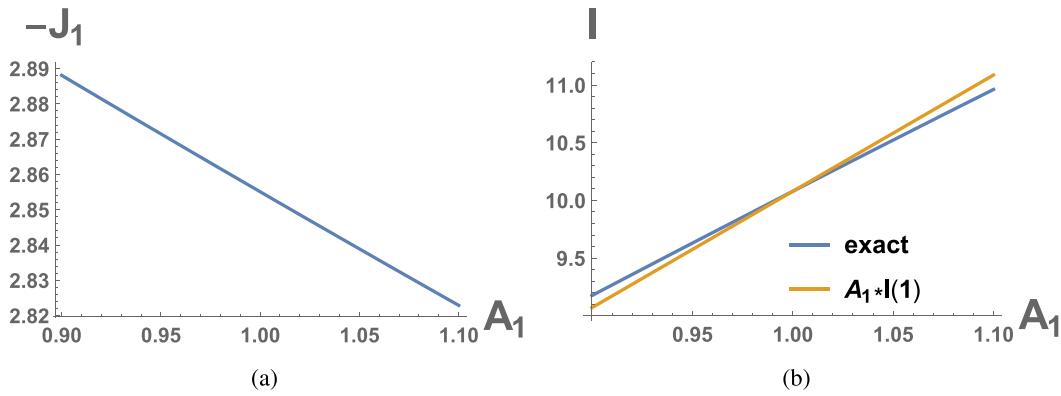

(a) (b)

FIG. 16. The dependence of flux $-J_1$ and current I on the parameter A_1.

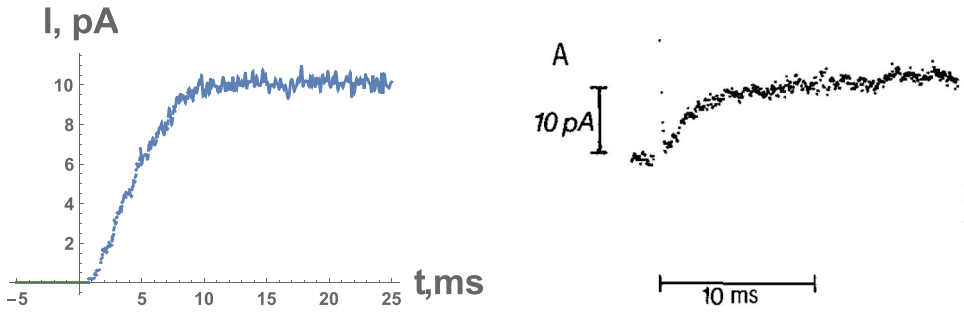

(a) (b)

FIG. 17. (a) The ensemble curves for the current I with 50 channels, where $s_{b0} \sim N(0, \sigma^2)$ and $A_1(t_i) \sim N(1, \sigma_A^2)$, with $\sigma = 0.05, \sigma_A = 0.03$. (b) The experimental curve from Fig. 2(a) in Llano *et al.* (1988).

bubble evolves. We take $A_1(t_i) \sim N(1, \sigma_A^2)$ with $\sigma_A = 0.03$ for each discrete time $t = t_i$ and for each channel. Figure 17(a) shows the ensemble curve for the current with 50 channels, where $s_{b0} \sim N(0, \sigma^2)$ and $A_1(t_i) \sim N(1, \sigma_A^2)$, with $\sigma = 0.05, \sigma_A = 0.03$, and 400 discrete t_i are used for the time interval of 30 ms. Figure 17(a) agrees well with the experimental results in Fig. 17(b), which is Fig. 2(a) in Llano *et al.* (1988). It also shows similar features and fluctuations with Fig. 2(c) in Llano *et al.* (1988) and Fig. 3.17 in Hille (2001).

To model the Cole–Moore delay (Cole & Moore, 1960; Hoshi & Armstrong, 2015), we can treat the mean value μ and standard variation σ as a function of the holding potential V_0. For illustration, we take

$$\begin{aligned} &s_{b0} \sim N(\mu, \sigma^2), \\ &\mu(V_0) = s \tanh(k(V_0 - V_0^*)), \quad V_0^* = -80\text{mV}, \quad k = 0.002/\text{mV}, \\ &\sigma(V_0) = \sigma_0 = 0.05 \end{aligned} \tag{4.2}$$

Downloaded from https://academic.oup.com/imamat/article/88/5/805/7589766 by guest on 28 March 2024

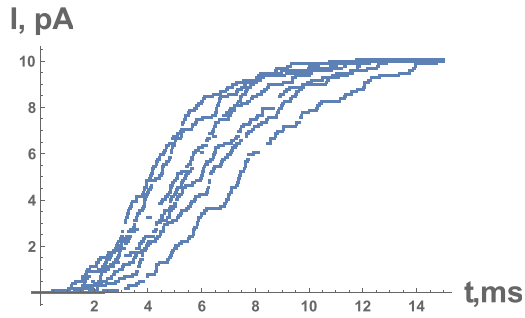

(a)

FIG. 18. The ensemble curves for the current with 100 channels and $V_0 + V_1 = 80$ mV, for seven different holding potential V_0= $[-52, -72, -93, -113, -133, -162, -212]$ mV, corresponding to curves from left to right.

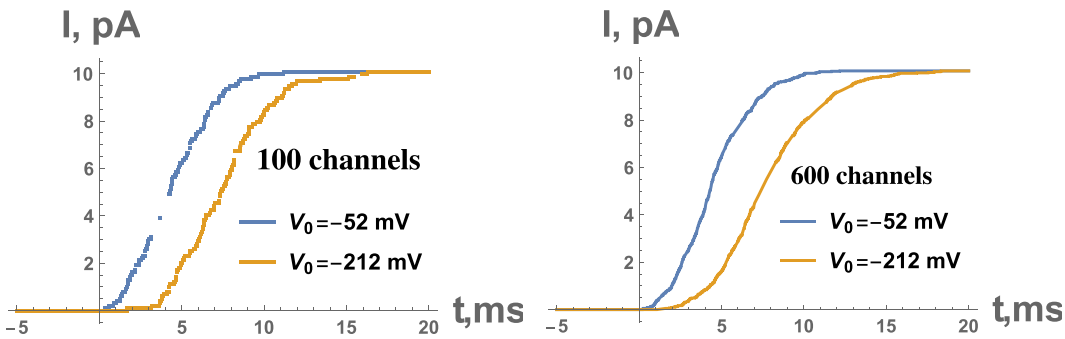

(a) (b)

FIG. 19. The ensemble curves for the current for $V_0 + V_1 = 80$ mV and two different holding potential V_0, (a) with 100 channels, and (b) with 600 channels.

where V_0 is the initial holding potential, and V_0^* is a reference value. Figure 18 shows the ensemble curves for the current with 100 channels and $V_0 + V_1 = 80$ mV, for seven different holding potential V_0 that are $[-52, -72, -93, -113, -133, -162, -212]$ mV, corresponding to curves from left to right. Figure 19 shows the ensemble curves for the current with 100 channels and 600 channels and with $V_0 + V_1 = 80$ mV, for two different holding potential $V_0 = -52, -212$ mV. It can be observed from the figures that the delay is longer when holding potential V_0 is smaller, while the overall shape of the ensemble curves does not change much.The ensemble curves show similar features as experimental curves in Cole & Moore (1960).

REMARK 7. As noted in Hoshi & Armstrong (2015), 'the mechanism of the Cole–Moore effect remains a mystery'. It is commonly shown in experiments and MD simulations (Bezanilla *et al.*, 1994; Jensen *et al.*, 2012; Aryal *et al.*, 2015; Priest *et al.*, 2021) that the gating current of the voltage sensor in the voltage sensor domain (VSD) is concurrent with the hydrophobic gating in the conduction pore (followed by ionic current). Therefore, many scientists believe that the voltage sensor plays a key role in the mechanism of Cole–Moore effect (Jensen *et al.*, 2010, 2012; Priest *et al.*, 2021). However, the linkage or functional coupling of VSD to conduction domain is less clear, e.g. various coupling mechanisms

Downloaded from https://academic.oup.com/imamat/article/88/5/805/7589766 by guest on 28 March 2024

have been proposed (Schow *et al.*, 2012; Carvalho-de Souza & Bezanilla, 2019; Bassetto *et al.*, 2021). The present work is an attempt of providing a possible mechanism of Cole–Moore effect directly from the conduction pore. It is also likely that the voltage sensor together with channel wall properties and conformational changes will have an impact on the positions and sizes of bubbles as modelled in (4.2). The detailed mechanism is left for future investigation.

5. Conclusion

In this paper, we present a macroscopic bubble model for the gating of K_v channels. The time delay in the opening of a single channel is determined by the motion of the bubble before it collapses. The bubble motion is coupled with a PNP system, which is solved by a full numerical computation as well as a quasi-static approximation method. We also present a stochastic model for the bubble and channel sizes and the ensemble properties of the K_v channel are consistent with experimental observations. Furthermore, the Cole–Moore delay is explored by assuming the dependence of bubble properties on the holding potential.

Although the present simple model captures some key features in the ensemble properties, some parts are oversimplified and there is room for improvement. The permanent charges in the channel are lumped together in the model, and the distinction and effects of charges on bubble and on the channel wall could be examined in the future. The selectivity of channel is not considered in detail here, which depends on the ion sizes (which makes the PNP system very complicated). This is circumvented by assuming small diffusion constants of other ions except K^+ in the present work. The generalization to high-dimensional case is also interesting and non-trivial, since the bubble interface will have a curved shape and specific forces (e.g. some force due to the maxwell stress) can act on the interface.

Funding

This work was partially supported by the National Natural Science Foundation of China (no. 12231004, 12071190) and Natural Sciences and Engineering Research Council of Canada (NSERC). We also would like to thank American Institute of Mathematics where this project was initiated.

References

Aryal, P., Sansom, M. S. P. & Tucker, S. J. (2015) Hydrophobic gating in ion channels. *J. Molecular Biol.*, **427**, 121–130.

Bassetto, C. A. Z., Souza, J. L. C.-D. & Bezanilla, F. (2021) Molecular basis for functional connectivity between the voltage sensor and the selectivity filter gate in shaker K+ channels. *Elife*, **10**, e63077.

Beckstein, O. & Sansom, M. S. P. (2003) Liquid–vapor oscillations of water in hydrophobic nanopores. *Proc. Natl. Acad. Sci.*, **100**, 7063–7068.

Beckstein, O. & Sansom, M. S. P. (2004) The influence of geometry, surface character, and flexibility on the permeation of ions and water through biological pores. *Phys. Biol.*, **1**, 42.

Bezanilla, F. (2008a) How membrane proteins sense voltage. *Nat. Rev. Mol. Cell Biol.*, **9**, 323–332 .

Bezanilla, F. (2008b) Ion channels: from conductance to structure. *Neuron*,**60**, 456–468.

Bezanilla, F. (2002) Voltage sensor movements. *J. Gen. Physiol.*, **120**, 465–473.

Bezanilla, F. (2018) Gating currents. *J. Gen. Physiol.*, **150**, 911–932.

Bezanilla, F., Perozo, E. & Stefani, E. (1994) Gating of shaker K+ channels: II. The components of gating currents and a model of channel activation. *Biophys. J.*, **66**, 1011–1021.

Biel, M., Wahl-Schott, C., Michalakis, S. & Zong, X. (2009) Hyperpolarization-activated cation channels: from genes to function. *Physiol. Rev.*, **89**, 847–885.

Downloaded from https://academic.oup.com/imamat/article/88/5/805/7589766 by guest on 28 March 2024

Boda, D., Nonner, W., Valisko, M., Henderson, D., Eisenberg, B. & Gillespie, D. (2007) Steric selectivity in na channels arising from protein polarization and mobile side chains. *Biophys. J.*, **93**, 1960–1980.

Cao, X., Song, Z., Horng, T.-L. & Huang, H. (2020) Electric potential generation of electrocytes: modelling, analysis, and computation. *J. Theor. Biol.*, **487**, 110107.

Carvalho-de Souza, J. L. & Bezanilla, F. (2019) Noncanonical mechanism of voltage sensor coupling to pore revealed by tandem dimers of shaker. *Nat. Commun.*, **10**, 1–12.

Catacuzzeno, L. & Franciolini, F. (2019) Simulation of gating currents of the shaker K channel using a Brownian model of the voltage sensor. *Biophys. J.*, **117**, 2005–2019.

Catacuzzeno, L., Franciolini, F., Bezanilla, F. & Eisenberg, R. S. (2021a) Gating current noise produced by brownian models of a voltage sensor. *Biophys. J.*, **120**, 3983–4001.

Catacuzzeno, L., Sforna, L. & Franciolini, F. (2020a) Voltage-dependent gating in K channels: experimental results and quantitative models. *Pflügers Arch*, **472**, 27–47.

Catacuzzeno, L., Sforna, L., Franciolini, F. & Eisenberg, R. (2020b) Why are voltage gated na channels faster than k channels? one multi-scale hierarchical model. bioRxiv Cold Spring Harbor Laboratory, p. 11.

Catacuzzeno, L., Sforna, L., Franciolini, F. & Eisenberg, R. S. (2021b) Multiscale modeling shows that dielectric differences make NaV channels faster than Kv channels. *J. Gen. Physio.*, **153**(2), e202012706.

Cole, K. S. & Moore, J. W. (1960) Potassium ion current in the squid giant axon: dynamic characteristic. *Biophys. J.*, **1**, 1–14.

Colquhoun, D. & Hawkes, A. G. (1981) On the stochastic properties of single ion channels. *Proc. R. Soc. Lond. Ser. B. Biol. Sci.*, **211**, 205–235.

Colquhoun, D. & Hawkes, A. G. (1995) The principles of the stochastic interpretation of ion-channel mechanisms. In: *Single-Channel Recording*. Springer, Boston, MA, pp. 397–482.

Delemotte, L., Kasimova, M. A., Sigg, D., Klein, M. L., Carnevale, V. & Tarek, M. (2017) Exploring the complex dynamics of an ion channel voltage sensor domain via computation. BioRxiv Cold Spring Harbor Laboratory, **108217** .

Delemotte, L., Tarek, M., Klein, M. L., Amaral, C. & Treptow, W. (2011) Intermediate states of the Kv1. 2 voltage sensor from atomistic molecular dynamics simulations. *Proc. Natl. Acad. Sci.*, **108**, 6109–6114.

Dryga, A., Chakrabarty, S., Vicatos, S. & Warshel, A. (2012) Coarse grained model for exploring voltage dependent ion channels. *Biochim. Biophys. Acta*, **1818**, 303–317.

Dudev, T. & Lim, C. (2010) Factors governing the na+vs k+ selectivity in sodium ion channels. *J. Am. Chem. Soc.*, **132**, 2321–2332.

Dudev, T. & Lim, C. (2014) Ion selectivity strategies of sodium channel selectivity filters. *Acc. Chem. Res.*, **47**, 3580–3587.

Eisenberg, B., Gold, N., Song, Z. & Huang, H. (2018) What current flows through a resistor? arXiv preprint arXiv:1805.04814.

Eisenberg, B. & Liu, W. (2007) Poisson–Nernst–Planck systems for ion channels with permanent charges. *SIAM J. Math. Anal.*, **38**, 1932–1966.

Eisenberg, B., Oriols, X. & Ferry, D. (2017) Dynamics of current, charge and mass. *Comput. Math. Biophys.*, **5**, 78–115.

Gould, S.J. (1987) *The Flamingo's Smile: Reflections in Natural History*. New York: Norton.

Hamill, O. P., Marty, A., Neher, E., Sakmann, B. & Sigworth, F. J. (1981) Improved patch-clamp techniques for high-resolution current recording from cells and cell-free membrane patches. *Pflügers Arch.*, **391**, 85–100.

Hille, B. (2001) *Ion Channels of Excitable Membranes*. Sinauer Associates, Inc, Sunderland, Massachusetts.

Hodgkin, A. L. (1992) *Chance and Design*. New York: Cambridge University Press.

Hodgkin, A., Huxley, A. & Katz, B. (1949) Ionic currents underlying activity in the giant axon of the squid. *Arch. Sci. Physiol.*, **3**, 129–150.

Hodgkin, A. L. & Huxley, A. F. (1952) A quantitative description of membrane current and its application to conduction and excitation in nerve. *The Journal of physiology*, **117**, 500.

Horng, T.-L., Eisenberg, R. S., Liu, C. & Bezanilla, F. (2016) Gating current models computed with consistent interactions. *Biophys. J.*, **110**, 102a–103a.

Downloaded from https://academic.oup.com/imamat/article/88/5/805/7589766 by guest on 28 March 2024

Horng, T.-L., Eisenberg, R. S., Liu, C. & Bezanilla, F. (2019) Continuum gating current models computed with consistent interactions. *Biophys. J.*, **116**, 270–282.

Hoshi, T. & Armstrong, C. M. (2015) The Cole-Moore effect: still unexplained? *Biophys. J.*, **109**, 1312–1316.

Huxley, A. F. (2002) From overshoot to voltage clamp. *Trends Neurosci.*, **25**, 553–558.

Huxley, A. F. (1963) The quantitative analysis of excitation and conduction in nerve. *Science*, **1963**, 242–260.

Huxley, A. F. (1996) *Kenneth Stewart Cole 1900–1984. A Biographical Memoir by Sir Andrew Huxley*. Washington, DC: National Academies Press.

Jacobson, D. A., Mendez, F., Thompson, M., Torres, J., Cochet, O. & Philipson, L. H. (2010) Calcium-activated and voltage-gated potassium channels of the pancreatic islet impart distinct and complementary roles during secretagogue induced electrical responses. *J. Physiol.*, **588**, 3525–3537.

Jensen, M. Ø., Borhani, D. W., Lindorff-Larsen, K., Maragakis, P., Jogini, V., Eastwood, M. P., Dror, R. O. & Shaw, D. E. (2010) Principles of conduction and hydrophobic gating in K+ channels. *Proc. Natl. Acad. Sci.*, **107**, 5833–5838.

Jensen, M. Ø., Jogini, V., Borhani, D. W., Leffler, A. E., Dror, R. O. & Shaw, D. E. (2012) Mechanism of voltage gating in potassium channels. *Science*, **336**, 229–233.

Kim, I. & Warshel, A. (2014) Coarse-grained simulations of the gating current in the voltage-activated Kv1.2 channel. *Proc. Natl. Acad. Sci.*, **111**, 2128–2133.

Lacroix, J. J., Hyde, H. C., Campos, F. V. & Bezanilla, F. (2014) Moving gating charges through the gating pore in a KV channel voltage sensor. *Proc. Natl. Acad. Sci.*, **111**, E1950–E1959.

Langan, P. S., Vandavasi, V. G., Kopec, W., Sullivan, B., Afonne, P. V., Weiss, K. L., de Groot, B. L. & Coates, L. (2020) The structure of a potassium-selective ion channel reveals a hydrophobic gate regulating ion permeation. *IUCrJ*, **7**, 835–843.

Lim, C. & Dudev, T. (2016) *Potassium Versus Sodium Selectivity in Monovalent Ion Channel Selectivity Filters*. Springer, Cham, pp. 325–347.

Llano, I. & Bookman, R. I. C. H. A. R. D. J. (1986) Ionic conductances of squid giant fiber lobe neurons. *J. Gen. Physiol.*, **88**, 543–569.

Llano, I., Webb, C. K. & Bezanilla, F. (1988) Potassium conductance of the squid giant axon. Single-channel studies. *J. Gen. Physiol.*, **92**, 179–196.

MacKinnon, R. (2004) Nobel lecture. Potassium channels and the atomic basis of selective ion conduction. *Biosci. Rep.*, **24**, 75–100.

Miedema, H., Vrouenraets, M., Wierenga, J., Meijberg, W., Robillard, G. & Eisenberg, B. (2007) A biological porin engineered into a molecular, nanofluidic diode. *Nano Lett.*, **7**, 2886–2891.

Moore, J. W. & Cole, K. S. (1960) Resting and action potentials of the squid giant axon in vivo. *J. Gen. Physiol.*, **43**, 961–970.

Neher, E. (1997) *Ion Channels for Communication Between and Within Cells Nobel Lecture, December 9, 1991, pages 10–25*. Singapore: World Scientific Publishing Co.

Peyser, A. & Nonner, W. (2012) Voltage sensing in ion channels: mesoscale simulations of biological devices. *Phys. Rev. E*, **86**, 011910.

Priest, M. F., Lee, E. E. & Bezanilla, F. (2021) Tracking the movement of discrete gating charges in a voltage-gated potassium channel. *Elife*, **10**, e58148.

Sakmann, B. & Neher, E. (1995) *Single Channel Recording*, 2nd edn. New York: Plenum.

Schoppa, N. E. & Sigworth, F. J. (1998) Activation of shaker potassium channels: I. Characterization of voltage-dependent transitions. *J. Gen. Physiol.*, **111**, 271–294.

Schow, E. V., Alfredo Freites, J., Nizkorodov, A., White, S. H. & Tobias, D. J. (2012) Coupling between the voltage-sensing and pore domains in a voltage-gated potassium channel. *Biochim. Biophys. Acta*, **1818**, 1726–1736.

Song, Z., Cao, X., Horng, T.-L. & Huang, H. (2019) Selectivity of the KcsA potassium channel: analysis and computation. *Phys. Rev. E*, **100**, 022406.

Song, Z., Cao, X., Horng, T.-L. & Huang, H. (2020) Electric discharge of electrocytes: modelling, analysis and simulation. *J. Theor. Biol.*, **498**, 110294.

Downloaded from https://academic.oup.com/imamat/article/88/5/805/7589766 by guest on 28 March 2024

Song, Z., Cao, X. & Huang, H. (2018) Electroneutral models for a multidimensional dynamic Poisson-Nernst-Planck system. *Phys. Rev. E*, **3)(98)**, 032404.
Taylor, R. E., Moore, J. W. & Cole, K. S. (1960) Analysis of certain errors in squid axon voltage clamp measurements. *Biophys. J.*, **1**, 161–202.
Tytgat, J. & Hess, P. (1992) Evidence for cooperative interactions in potassium channel gating. *Nature*, **359**, 420–423.
Werry, D., Eldstrom, J., Wang, Z. & Fedida, D. (2013) Single-channel basis for the slow activation of the repolarizing cardiac potassium current, IKs. *Proc. Natl. Acad. Sci.*, **110**, E996–E1005.
Zhang, L. & Liu, W. (2020) Effects of large permanent charges on ionic flows via poisson–nernst–planck models. *SIAM J. Appl. Dyn. Syst.*, **19**, 1993–2029.
Zheng, J. & Trudeau, M. C. (2015) *Handbook of Ion Channels*. CRC Press, Boca Raton, FL.

A. Parameter values

We adopt the following values for the physical parameters (Llano & Bookman, 1986; Llano *et al.*, 1988)

$$\begin{aligned}
&L = 0.75\text{nm}, \quad s = 0.15\text{nm}, \quad A = (0.7\text{nm})^2, \quad c_0 = 560\,\text{mM} \approx 3.37 \times 10^{26}/\text{m}^3,\\
&c_1^L = 10\text{mM}, \quad c_2^L = 550\text{mM}, \quad c_3^L = 560\text{mM},\\
&c_1^R = 400\text{mM}, \quad c_2^R = 160\text{mM}, \quad c_3^R = 560\text{mM},\\
&D_0 = D_1 = 10^{-10}\text{m}^2/\text{s}, \quad D_2 = D_3 = 10^{-12}\text{m}^2/\text{s}, D_b = 10^{-19}\text{m}^2/\text{s},\\
&AJ_0 = AD_0c_0/L \approx 2.2 \times 10^7/\text{s}, \quad e_0AJ_0 \approx 3.53\,\text{pA},\\
&t_0 = \frac{L^2}{D_0} = 5.625 \times 10^{-9}\text{s}, \quad V_0 = -80\text{mV}, \quad V_1 = 160\text{mV}.
\end{aligned} \tag{A.1}$$

The dimensionless quantities are

$$\begin{aligned}
&\varepsilon = \frac{\varepsilon_0 k_B T}{e_0^2 c_0 L^2} \approx 7.3 \times 10^{-3}, \quad \beta = LAc_0 \approx 0.12,\\
&c_1^L \approx 0.018, \quad c_2^L \approx 0.982, \quad c_3^L = 1,\\
&c_1^R \approx 0.71, \quad c_2^R \approx 0.29, \quad c_3^R = 1,\\
&D_1 = 1, \quad D_2 = D_3 = 0.01, \quad D_b = 10^{-9},\\
&V_0 = -3.18, \quad V_1 = 6.36.
\end{aligned} \tag{A.2}$$

B. Continuity of the total current

B.1 *The continuous system*

The total current consists of three different forms of current in different regions

(i) the current from the change of electric field (for the whole interval/channel);

(ii) the current from the ionic fluxes (outside of the bubble);

(iii) the current from the motion of the bubble charge (in the bubble).

Downloaded from https://academic.oup.com/imamat/article/88/5/805/7589766 by guest on 28 March 2024

We will illustrate the continuity of the total current by the dimensional system in Section 2.1. For the region outside of the bubble ($-L < x < s_b, s < x < L$), we define the total current (per unit cross-sectional area) as I^{pnp}_{total}:

$$I^{pnp}_{total}(x,t) = \varepsilon_0\varepsilon_r\partial_t E + \sum_{i=1}^{3} e_0 z_i J_i = -\varepsilon_0\varepsilon_r\partial_{tx}\phi + e_0(J_1 + J_2 - J_3). \tag{B.1}$$

Taking the time derivative of $(2.2)_1$ and using $(2.2)_2$, we obtain

$$\partial_x I^{pnp}_{total} = 0, \tag{B.2}$$

which implies the continuity of current outside of the bubble.

In the bubble, the define the total current (per unit cross-sectional area) as

$$I^{bubble}_{total}(x,t) = \varepsilon_0\varepsilon_r\partial_t E + \partial_t Q_b = -\varepsilon_0\varepsilon_r\partial_{tx}\phi - \partial_t Q_b, \tag{B.3}$$

where Q_b is the total bubble charge (per unit area) stored in the interval $[s_b, x]$ (it is the magnitude of total negative charge)

$$Q_b = \int_{s_b}^{x} \frac{q_b}{V_b} dx = \frac{q_b(x - s_b)}{A(s - s_b)}. \tag{B.4}$$

If Q_b increases, it means some positive current of the bubble charge goes across the interface at x. Another interpretation is based on the velocity of the cross-sectional surface at x

$$v(x) = \frac{(s - x)}{(s - s_b)} \frac{ds_b}{dt}, \tag{B.5}$$

and one can easily verify that

$$\partial_t Q_b = J_b = -\frac{q_b}{V_b} v(x). \tag{B.6}$$

Taking the time derivative of (2.3), we obtain the continuity of the total current in the bubble

$$\partial_x I^{bubble}_{total} = 0. \tag{B.7}$$

B.2 *The discrete numerical scheme*

The quantities q_k^{n+1} and $\varepsilon_{r,k+1/2}$ are defined as

$$q_k^{n+1} = \int_{x_{k-1/2}}^{x_{k+1/2}} \frac{1}{\beta} \frac{q_b}{(s - s_b)} dx, \tag{B.8}$$

Downloaded from https://academic.oup.com/imamat/article/88/5/805/7589766 by guest on 28 March 2024

and

$$\varepsilon_{r,k+1/2} = \frac{h}{\frac{h_1}{\varepsilon_{r1}} + \frac{h_2}{\varepsilon_{r0}}}, \quad h_1 = s_b - x_k, \quad h_2 = x_{k+1} - s_b, \quad \text{if } s_b \in [x_k, x_{k+1}]. \tag{B.9}$$

Next we show the continuity of the total current in the discrete scheme. The equation of ϕ can be written as

$$\begin{aligned} &J^{n+1}_{\phi,k+1/2} - J^{n+1}_{\phi,k-1/2} = hc^{n+1}_{1,k} + hc^{n+1}_{2,k} - hc^{n+1}_{3,k} + hq^{n+1}_k, \\ &J^{n+1}_{\phi,k+1/2} = -\varepsilon\varepsilon_{r,k+1/2}\frac{\phi^{n+1}_{k+1} - \phi^{n+1}_k}{h}. \end{aligned} \tag{B.10}$$

Summing over $k = 1, .., N$ gives

$$J^{n+1}_{\phi,N+1/2} - J^{n+1}_{\phi,1/2} = h\sum_{k=1}^{N} c^{n+1}_{1,k} + \sum_{k=1}^{N} hc^{n+1}_{2,k} - \sum_{k=1}^{N} hc^{n+1}_{3,k} + \sum_{k=1}^{N} hq^{n+1}_k. \tag{B.11}$$

Repeat it for J^n with the time step t_n, take the difference, divide it by Δt, and then we obtain

$$\begin{aligned} &\frac{J^{n+1}_{\phi,N+1/2} - J^{n}_{\phi,N+1/2}}{\Delta t} - \frac{J^{n+1}_{\phi,1/2} - J^{n}_{\phi,1/2}}{\Delta t} \\ =&h\sum_{k=1}^{N}\frac{c^{n+1}_{1,k} - c^{n}_{1,k}}{\Delta t} + h\sum_{k=1}^{N}\frac{c^{n+1}_{2,k} - c^{n}_{2,k}}{\Delta t} - h\sum_{k=1}^{N}\frac{c^{n+1}_{3,k} - c^{n}_{3,k}}{\Delta t} \\ &+ \frac{h}{\Delta t}\left(\sum_{k=1}^{N} q^{n+1}_k - \sum_{k=1}^{N} q^{n}_k\right) \\ =&-\left(J^{n+1}_{1,N+1/2} - J^{n+1}_{1,1/2}\right) - \left(J^{n+1}_{2,N+1/2} - J^{n+1}_{2,1/2}\right) + \left(J^{n+1}_{3,N+1/2} - J^{n+1}_{3,1/2}\right) \\ &+ \frac{h}{\Delta t}\left(Q^{n+1}_b - Q^{n}_b\right). \end{aligned} \tag{B.12}$$

Rearranging the terms leads to

$$\begin{aligned} &\frac{J^{n+1}_{\phi,N+1/2} - J^{n}_{\phi,N+1/2}}{\Delta t} + \left(J^{n+1}_{1,N+1/2} + J^{n+1}_{2,N+1/2} - J^{n+1}_{3,N+1/2}\right) - \frac{h}{\Delta t}\left(Q^{n+1}_b - Q^{n}_b\right) \\ =&\frac{J^{n+1}_{\phi,1/2} - J^{n}_{\phi,1/2}}{\Delta t} + J^{n+1}_{1,1/2} + J^{n+1}_{2,1/2} - J^{n+1}_{3,1/2}, \end{aligned} \tag{B.13}$$

where the three terms on the left-hand side are the discrete version of the three forms of currents defined in (i), (ii), (iii) in the previous subsection. If the sum is over the entire interval (i.e. $N + 1/2$ is the right end), the term $Q^{n+1}_b - Q^n_b$ disappears since the total bubble charge Q^n_b is conserved by definition, and the total current is conserved at the two ends.

Downloaded from https://academic.oup.com/imamat/article/88/5/805/7589766 by guest on 28 March 2024

C. Derivation for quasi-static and steady state

C.1 *The quasi-static state*

For the quasi-static state, we ignore the dipole and V_0 (equivalently the ϕ is shifted up by a constant V_0 and continuity condition of ϕ will be used at interface). We first consider the right part $s < x < 1$. We obtain

$$\begin{aligned} &c_1 = c_1^R e^{-(\phi - V_1)}, \quad c_2 = c_2^R e^{-(\phi - V_1)}, \quad c_3 = e^{\phi - V_1}, \\ &\varepsilon\varepsilon_{r1}\phi'' = e^{\phi - V_1} - e^{-(\phi - V_1)}, \end{aligned} \tag{C.1}$$

where $c_3^R = c_1^R + c_2^R = 1$ have been used. Integrating once gives

$$\frac{1}{2}\varepsilon\varepsilon_{r1}[(\phi'(x))^2 - (\phi'(s+))^2] = e^{\phi - V_1} + e^{-(\phi - V_1)} - B_2, \tag{C.2}$$

where

$$B_2 = e^{\phi_s - V_1} + e^{-(\phi_s - V_1)}, \quad \phi'(s+) = \frac{\varepsilon_{r0}}{\varepsilon_{r1}}\phi'(s-) = \frac{\varepsilon_{r0}}{\varepsilon_{r1}}\tilde{\phi}_s. \tag{C.3}$$

Then, we obtain

$$(\phi'(x))^2 = G_1(\phi; \phi_s, \tilde{\phi}_s) = \left(\frac{\varepsilon_{r0}}{\varepsilon_{r1}}\tilde{\phi}_s\right)^2 + \frac{2}{\varepsilon\varepsilon_{r1}}[e^{\phi - V_1} + e^{-(\phi - V_1)} - B_2] \tag{C.4}$$

and

$$x = \int_{\phi_s}^{\phi} \frac{1}{\sqrt{G_1(\phi; \phi_s, \tilde{\phi}_s)}} d\phi + s. \tag{C.5}$$

For the left part $-1 < x < s_b$, we obtain

$$\begin{aligned} &\varepsilon\varepsilon_{r1}\phi'' = e^{\phi} - e^{-\phi}, \\ &\frac{1}{2}\varepsilon\varepsilon_{r1}[(\phi'(x))^2 - (\phi'(s_b-))^2] = e^{\phi} + e^{-\phi} - B_3, \end{aligned} \tag{C.6}$$

with

$$\begin{aligned} &B_3 = e^{\phi_{s_b}} + e^{-\phi_{s_b}}, \quad \phi_{s_b} = B_1(s_b - s)^2 + \tilde{\phi}_s(s_b - s) + \phi_s \\ &\phi'(s_b-) = \frac{\varepsilon_{r0}}{\varepsilon_{r1}}\phi'(s_b+) = \frac{\varepsilon_{r0}}{\varepsilon_{r1}}[\tilde{\phi}_s + 2B_1(s_b - s)], \end{aligned} \tag{C.7}$$

Downloaded from https://academic.oup.com/imamat/article/88/5/805/7589766 by guest on 28 March 2024

where B_1 is given in (3.16). Then, we obtain

$$(\phi'(x))^2 = G_2(\phi;\phi_s,\tilde{\phi}_s) = (\phi'(s_b-))^2 + \frac{2}{\varepsilon\varepsilon_{r1}}[e^{\phi} + e^{-\phi} - B_3] \tag{C.8}$$

and

$$x = -\int_{\phi_{s_b}}^{\phi} \frac{1}{\sqrt{G_2(\phi;\phi_s,\tilde{\phi}_s)}} d\phi + s_b. \tag{C.9}$$

C.2 *The steady state*

Now we consider the steady state. Define

$$p = c_1 + c_2, \quad J_p = J_1 + \frac{J_2}{D_2}, \tag{C.10}$$

then the two equations for c_1 and c_2 lead to

$$-J_p = p'(x) + p\phi'(x). \tag{C.11}$$

Let $V = V_0 + V_1$. For the right part $x > s$, we obtain

$$c_3 = c_3^R e^{\phi - V} = e^{\phi - V}. \tag{C.12}$$

Multiplying ϕ' in the equation of ϕ (i.e. equation $(3.21)_1$, and the delta function is put into the jump conditions) gives

$$-\varepsilon\varepsilon_{r1}\phi''(x)\phi'(x) = p\phi' - c_3\phi' = -J_p - p' - c_3', \tag{C.13}$$

and integrating gives

$$p = \frac{1}{2}\varepsilon\varepsilon_{r1}\left[(\phi'(x))^2 - (\phi'(1))^2\right] - J_p(x-1) - c_3 + 2, \tag{C.14}$$

where the boundary conditions at $x = 1$ have been used. Substituting into $(3.21)_1$, we obtain

$$-\varepsilon\varepsilon_{r1}\phi''(x) = \frac{1}{2}\varepsilon\varepsilon_{r1}\left[(\phi'(x))^2 - (\phi'(1))^2\right] - J_p(x-1) - 2(e^{\phi - V} - 1), \tag{C.15}$$

for $x > s$. Similarly for the left part $x < s$, we have

$$\begin{aligned} c_3 = c_3^L e^{\phi}, \quad c_1 = \frac{1}{2}\varepsilon\varepsilon_{r1}\left[(\phi'(x))^2 - (\phi'(-1))^2\right] - J_p(x+1) - c_3 + 2, \\ -\varepsilon\varepsilon_{r1}\phi''(x) = \frac{1}{2}\varepsilon\varepsilon_{r1}\left[(\phi'(x))^2 - (\phi'(-1))^2\right] - J_p(x+1) - 2(e^{\phi} - 1). \end{aligned} \tag{C.16}$$

Downloaded from https://academic.oup.com/imamat/article/88/5/805/7589766 by guest on 28 March 2024